



Global combustion sources of organic aerosols: model comparison with 84 AMS factor-analysis data sets

Alexandra P. Tsimpidi¹, Vlassis A. Karydis¹, Spyros N. Pandis^{2,3}, and Jos Lelieveld^{1,4}

¹Max Planck Institute for Chemistry, Mainz, Germany

²Department of Chemical Engineering, University of Patras, Patras, Greece

³Department of Chemical Engineering, Carnegie Mellon University, Pittsburgh, PA, USA

⁴Energy, Environment and Water Research Center, Cyprus Institute, Nicosia, Cyprus

Correspondence to: Alexandra P. Tsimpidi (a.tsimpidi@mpic.de)

Received: 8 December 2015 – Published in Atmos. Chem. Phys. Discuss.: 3 February 2016

Revised: 30 May 2016 – Accepted: 20 June 2016 – Published: 20 July 2016

Abstract. Emissions of organic compounds from biomass, biofuel, and fossil fuel combustion strongly influence the global atmospheric aerosol load. Some of the organics are directly released as primary organic aerosol (POA). Most are emitted in the gas phase and undergo chemical transformations (i.e., oxidation by hydroxyl radical) and form secondary organic aerosol (SOA). In this work we use the global chemistry climate model ECHAM/MESSy Atmospheric Chemistry (EMAC) with a computationally efficient module for the description of organic aerosol (OA) composition and evolution in the atmosphere (ORACLE). The tropospheric burden of open biomass and anthropogenic (fossil and biofuel) combustion particles is estimated to be 0.59 and 0.63 Tg, respectively, accounting for about 30 and 32 % of the total tropospheric OA load. About 30 % of the open biomass burning and 10 % of the anthropogenic combustion aerosols originate from direct particle emissions, whereas the rest is formed in the atmosphere. A comprehensive data set of aerosol mass spectrometer (AMS) measurements along with factor-analysis results from 84 field campaigns across the Northern Hemisphere are used to evaluate the model results. Both the AMS observations and the model results suggest that over urban areas both POA (25–40 %) and SOA (60–75 %) contribute substantially to the overall OA mass, whereas further downwind and in rural areas the POA concentrations decrease substantially and SOA dominates (80–85 %). EMAC does a reasonable job in reproducing POA and SOA levels during most of the year. However, it tends to underpredict POA and SOA concentrations during winter indicating that the model misses wintertime sources of OA (e.g., residential

biofuel use) and SOA formation pathways (e.g., multiphase oxidation).

1 Introduction

Organic aerosol (OA) is a major contributor to fine particulate matter mass with potentially harmful effects on the environment and human health (Lelieveld et al., 2013; Poschl, 2005); however, the sources are poorly understood (Kanakidou et al., 2005; Goldstein and Galbally, 2007; Donahue et al., 2009; Tsigaridis et al., 2014). OA comprises primary organic aerosol (POA), i.e., directly emitted in the particulate phase, and secondary organic aerosol (SOA), formed within the atmosphere from the oxidation of gas-phase precursors. POA constitutes the particulate OA fraction emitted by anthropogenic combustion processes (i.e., fossil fuels, biofuels) and open biomass burning (i.e., savanna and forest fires). Anthropogenic combustion emissions of particulate organic carbon (OC) are estimated at $13.9 \text{ Tg C yr}^{-1}$ for the year 2005 (Clarke et al., 2007). OC emissions from open biomass burning range from 13.5 to $21.4 \text{ Tg C yr}^{-1}$ during the decade since 2000 (van der Werf et al., 2010). POA emitted from combustion sources can evaporate rapidly during atmospheric dilution depending on ambient concentrations (Robinson et al., 2010; Ranjan et al., 2012; May et al., 2014). The phase partitioning of the emitted POA depends on the volatility distribution of the emissions. This distribution includes low volatility (LVOC; $C^* < 0.32 \mu\text{g m}^{-3}$), semivolatile (SVOC;

$0.32 \mu\text{g m}^{-3} < C^* < 320 \mu\text{g m}^{-3}$), and intermediate volatility (IVOC; $3.2 \times 10^2 \mu\text{g m}^{-3} < C^* < 3.2 \times 10^6 \mu\text{g m}^{-3}$) organic compounds. The corresponding emission factors can be measured using dilution samplers and are estimated as a function of the saturation concentration of the emitted organic compounds (Grieshop et al., 2009). Traditional emission inventories (e.g., Clarke et al., 2007; van Der Werf et al., 2010) account for only a small fraction of the emitted IVOCs since they are based on filter samples collected at aerosol concentrations up to $10^4 \mu\text{g m}^{-3}$ (Shrivastava et al., 2008; Robinson et al., 2010). The amount of IVOC emissions missing in traditional inventories is estimated to be between 0.25 and 2.8 times POA emissions, depending on the type of the source (Shrivastava et al., 2008; Robinson et al., 2010).

Organic emissions further downwind mix with background air, resulting in cooling and dilution and altering the gas-particle partitioning. The organic compounds that remain in the gas phase can undergo chemical transformations (i.e., oxidation by hydroxyl radical), become less volatile and may be transferred into SOA (Donahue et al., 2006). Therefore, in addition to direct emissions of POA, it is important to understand the potential of combustion emissions to contribute to SOA formation. Numerous studies have indicated that SOA usually exceeds POA even in urban environments with substantial primary emissions (Jimenez et al., 2009; Stone et al., 2009; Sun et al., 2011; Mohr et al., 2012; Hayes et al., 2013). However, the overall contribution of combustion emissions to ambient SOA and OA remains uncertain (Chirico et al., 2010; Miracolo et al., 2011; Samy and Zielinska, 2010; Gentner et al., 2012; Bahreini et al., 2012; Gordon et al., 2014). Together with the OA mass concentration, the hygroscopic, chemical and optical properties continue to change because of chemical processing by gas-phase oxidants (Jimenez et al., 2009). These changes affect the OA radiative forcing on climate by direct and indirect effects, the latter through cloud formation (Poschl, 2005; McFiggans et al., 2006; IPCC; 2013).

Mass spectrometry has been widely used in aerosol analyses because of the universal, sensitive, and rapid detection of aerosol components (Suess and Prather, 1999). The aerosol mass spectrometer (AMS) (Jimenez et al., 2003) has been the most commonly used instrument in recent years. AMS is capable of quantitatively measuring the OA mass concentrations with high time and particle size resolution (Takegawa et al., 2005; Zhang et al., 2005b). Several factor-analysis techniques have been employed to extract information about processes and sources of OA. These techniques include principal component analysis (CPCA; Zhang et al., 2005a), multiple component analysis (MCA; Zhang et al., 2007), hierarchical cluster analysis (Marcolli et al., 2006), the multilinear engine (ME-2; Lanz et al., 2008), and positive matrix factorization (PMF; Paatero and Tapper, 1994; Paatero, 1997), with the latter being the most commonly used (Lanz et al., 2007; Nemitz et al., 2008; Aiken et al., 2009; Ulbrich et al., 2009; DeCarlo

et al., 2010; Mohr et al., 2012; Hayes et al., 2013; Crippa et al., 2014; Carbone et al., 2014; Chen et al., 2015).

PMF allows for the classification of OA into several types based on different temporal and mass spectral signatures. Two major components often resolved by the analysis of the AMS measurements are hydrocarbon-like organic aerosol (HOA) and oxygenated organic aerosol (OOA) (Zhang et al., 2007; Jimenez et al., 2009). Biomass burning OA (BBOA), marine-related OA (MOA), and cooking OA (COA) are other OA components that PMF may identify as important components of the observed OA (Lanz et al., 2010; Mohr et al., 2012; Kostenidou et al., 2013; Crippa et al., 2013a). HOA correlates with combustion tracers (e.g., CO, elemental carbon, and NO_x) and is considered as a surrogate for fossil fuel combustion POA (Lanz et al., 2007; Ulbrich et al., 2009; Crippa et al., 2014). BBOA correlates with tracers from biomass burning (e.g., acetonitrile, levoglucosan, and potassium) and is considered a surrogate of biomass burning POA (Aiken et al., 2010; Lanz et al., 2010; Crippa et al., 2014). OOA often correlates with secondary pollutants (e.g., ozone, sulfate, and nitrate) and is considered a surrogate for SOA (Jimenez et al., 2009; Ng et al., 2011). However, Crippa et al. (2014) have reported that the OOA correlation with secondary inorganic species might not be very high in at least some field campaigns. OOA can include SOA from various precursors, such as anthropogenic and biogenic volatile organic compounds (VOCs), as well as SVOCs and IVOCs from fossil fuel, biofuel, and open biomass burning. PMF often classifies OOA into two subtypes that differ in the degree of oxidation: a more strongly oxygenated low-volatility OOA (LV-OOA) often correlating with sulfate, and a less oxygenated semivolatile OOA (SV-OOA) usually correlating with nitrate (Jimenez et al., 2009; Crippa et al., 2014). Field campaigns in the Northern Hemisphere have shown that HOA accounts for approximately one-third of the OA in urban sites and OOA accounts for the remaining two-thirds, while OOA represents roughly 95 % of the OA in rural/remote regions (Zhang et al., 2007).

Global chemistry climate and chemical transport models systematically underpredict OA levels, especially over and downwind of anthropogenic source regions (Tsigaridis et al., 2014). At the same time, global models tend to predict a dominance of POA at mid-latitudes in the Northern Hemisphere while measurements indicate the opposite (Henze et al., 2008; Tsigaridis et al., 2014). The same models indicate that the formation of SOA from biogenic sources greatly exceeds that from anthropogenic sources. The shortcomings in many OA models are partially due to the assumption that POA is non-volatile and nonreactive (Kanakidou et al., 2005; Jimenez et al., 2009). To address these shortcomings, Donahue et al. (2006) developed the volatility basis set (VBS) framework, which assumes that POA emissions are semivolatile and photochemically reactive and uses logarithmically spaced volatility bins to distribute POA upon emission. Recently, several regional-scale modeling studies

have accounted for the semivolatile nature and chemical aging of organic compounds demonstrating improvements in reproducing the OA concentrations and chemical composition (Robinson et al., 2007; Shrivastava et al., 2008; Murphy and Pandis, 2009; Tsimpidi et al., 2010, 2011; Hodzic et al., 2010; Fountoukis et al., 2011, 2014; Bergström et al., 2012; Athanasopoulou et al., 2013; Zhang et al., 2013). However, only few global modeling studies have yet adopted the VBS approach to simulate the SOA formation from the chemical aging of SVOC and IVOC emissions (Jathar et al., 2011; Tsimpidi et al., 2014; Shrivastava et al., 2015; Hodzic et al., 2016). According to these studies, the modeled tropospheric burden of POA is 0.09–0.94 Tg and of SOA 1.8–2.8 Tg.

In this work we use ORACLE, a computationally efficient module for the description of organic aerosol composition and evolution in the atmosphere (Tsimpidi et al., 2014), to estimate the impact of open biomass burning and anthropogenic combustion emissions and their chemical aging on global OA budgets and distributions. An extensive global data set of AMS measurements and factor-analysis results from 84 field campaigns in the Northern Hemisphere are used in combination with the model results during the period of 2001–2010. This integrated effort provides further insights into the temporal and geographical variability of the OA particles, emission strengths and the chemical processing of organics from combustion sources.

2 Model description and application

2.1 EMAC model

The ECHAM/MESSEy Atmospheric Chemistry (EMAC) model is a numerical chemistry and climate simulation system that includes sub-models describing the lower and middle atmosphere processes (Jöckel et al., 2006). EMAC includes submodels that describe gas-phase chemistry (MECCA; Sander et al., 2011), inorganic aerosol microphysics (GMXe; Pringle et al., 2010), cloud microphysics (CLOUD; Jöckel et al., 2006), aerosol optical properties (AEROPT; Lauer et al., 2007), dry deposition (DRYDEP; Kerkweg et al., 2006a), sedimentation (SEDI; Kerkweg et al., 2006a), cloud scavenging (SCAV; Tost et al., 2006), emissions (ONLEM and OFFLEM; Kerkweg et al., 2006b), and organic aerosol formation and growth (ORACLE; Tsimpidi et al., 2014).

The removal of gas and aerosol organic compounds through dry deposition is calculated with the DRYDEP submodel (Kerkweg et al., 2006a) based on the big-leaf approach, and the dry deposition velocities depend on physical and chemical properties of the surface cover (e.g., the roughness length, soil pH, leaf stomatal exchange). The sedimentation of aerosols is calculated with the SEDI submodel (Kerkweg et al., 2006a) using a first-order trapezoid scheme. In-cloud scavenging and rainout of gas and aerosol species

are treated by the SCAV submodel (Tost et al., 2006). The effective Henry's law coefficient used for calculating the scavenging rates of LVOCs, SVOCs, and IVOCs is 10^5 M atm^{-1} .

The spectral resolution used in this study is T63L31, corresponding to a horizontal grid resolution of $1.875^\circ \times 1.875^\circ$ and 31 vertical layers extending to 10 hPa at about 25 km altitude. EMAC has been run for 11 years, covering the period 2000–2010, and the first year is used as spin-up. EMAC has been extensively described and evaluated against in situ observations and satellite measurements that include filter-based particulate matter concentrations, aerosol optical depth, acid deposition, gas-phase mixing ratios, and meteorological parameters (Jöckel et al., 2006; Pozzer et al., 2012a, b; Karydis et al., 2016). Tsimpidi et al. (2014) performed an in-depth evaluation of the EMAC calculated total OA over different continents by using measurements from the EMEP network over Europe, the IMPROVE network over North America, and several short-term field campaigns over East Asia, subtropical West Africa, the Amazon rainforest, and the Canadian boreal forest. The present work focuses on the model evaluation for the individual OA components (i.e., POA and SOA). In addition, the statistical evaluation of EMAC results for the inorganic components summarized in Tables S1–S3 in the Supplement.

2.2 ORACLE module

ORACLE is a computationally efficient submodel for the description of OA composition and evolution in the atmosphere, which has been implemented into the EMAC model by Tsimpidi et al. (2014). ORACLE simulates a variety of semivolatile organic species and reaction products and separates them into groups of compounds with logarithmically spaced effective saturation concentrations.

In this study, primary organic emissions from open biomass burning and from anthropogenic sources (i.e., fossil fuel and biofuel) are simulated using separate surrogate species for each source category. They are subdivided into three groups of organic compounds: LVOCs ($10^{-2} \mu\text{g m}^{-3}$), SVOCs (10^0 and $10^2 \mu\text{g m}^{-3}$), and IVOCs (10^4 and $10^6 \mu\text{g m}^{-3}$). These organic compounds are allowed to partition between the gas and aerosol phases resulting in the formation of fPOA (anthropogenic POA from fossil fuel and biofuel combustion) and bbPOA (natural POA from open biomass burning). VOCs are distinguished into anthropogenic and biogenic and their oxidation products are distributed in four volatility bins with effective saturation concentrations of 10^0 , 10^1 , 10^2 , and $10^3 \mu\text{g m}^{-3}$ at 298 K by using the aerosol mass yields (Table S4) by Tsimpidi et al. (2014). Gas-phase photochemical reactions that change the volatility of the organics are taken into account and their oxidation products (SOA-sv, SOA-iv, and SOA-v) are simulated separately in the module to keep track of their origin. The suffixes -sv, -iv and -v to the term SOA define a category of precursors (SVOCs, IVOCs, and VOCs, respec-

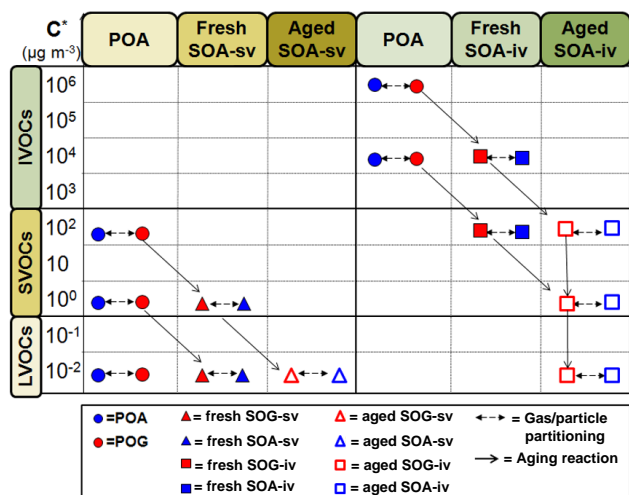
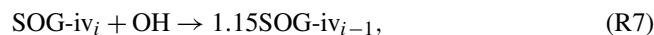
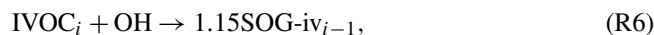


Figure 1. Schematic of the VBS resolution and the formation of SOA from SVOC and IVOC emissions. Red indicates the vapor phase and blue the particulate phase. The circles represent primary organic material that can be emitted either in the gas or in the aerosol phase. Filled triangles and squares indicate the formation of SOA from SVOCs and IVOCs, respectively, by fuel combustion and biomass burning sources from the first oxidation step (fresh SOA). Open triangles and squares represent SOA formed in additional oxidation steps (aged SOA) from SVOCs and IVOCs by the same sources. The partitioning processes, the aging reactions of the organic compounds, and the names of the species used to track all compounds are also shown.

tively). For the current application, SOA components are divided into four groups based on their source: anthropogenic from fossil fuel and biofuel combustion sources (fSOA), natural from open biomass burning (bbSOA), SOA from anthropogenic (aSOA-v) and biogenic (bSOA-v) VOCs. This study focuses on the OA produced from primary combustion sources and discusses in detail results for the first two types of SOA (fSOA and bbSOA). The model set up for simulating the formation of aSOA-v and bSOA-v and the corresponding results can be found in Tsimpidi et al. (2014). In addition, in this work ORACLE has been modified to distinguish the formation of fresh SOA and aged SOA by adding additional tracers to the model. The first generation oxidation products of SVOCs, IVOCs, and VOCs are characterized as fresh while SOA produced from any additional oxidation step is grouped together and considered aged (Fig. 1). LVOCs are not allowed to participate in photochemical reactions since they are in the lowest volatility bin. This assumption may introduce a small bias in our results only under extremely clean conditions ($OA \leq 10^{-2} \mu\text{g m}^{-3}$) where part of LVOC is in the gas phase. Adding another bin in the volatility distribution to accurately represent the extremely low-volatility organic compounds (e.g., ELVOCs with C^* lower than 10^{-3}) would be useful only for studying new particle formation, which is outside the scope of the current work.

The volatilities of SVOCs and IVOCs are reduced by a factor of 10^2 as a result of the OH reaction with a rate constant of $2 \times 10^{-11} \text{ cm}^3 \text{ molecule}^{-1} \text{ s}^{-1}$ and a 15 % increase in mass is assumed to account for two added oxygen atoms (Tsimpidi et al., 2014). This formulation is comparable to a number of global and regional studies, which assume 2 orders of magnitude reduction in volatility and up to 50 % increase in mass per reaction (e.g., Grieshop et al. 2009; Hodzic et al., 2010; Pye and Seinfeld, 2010). Shrivastava et al. (2011) even used 7 orders of magnitude reduction in volatility per reaction. However, despite the fact that most of the studies assume that each oxidation reaction of SVOC and IVOC reduces the volatility of the precursor by 1 (e.g., Tsimpidi et al., 2010; Jathar et al., 2011; Bergström et al., 2012) or 2 orders of magnitude, the oxidation products can be up to 4 orders of magnitude lower in volatility than the precursor (Kroll and Seinfeld, 2008). Furthermore, ORACLE calculates the fraction of the semivolatile organic compounds that condenses to (or evaporates from) the particle phase by assuming bulk equilibrium and that all organic compounds form a pseudo-ideal solution (Tsimpidi et al., 2014). Overall, the primary aerosol formation from the phase partitioning of the freshly emitted LVOCs and SVOCs, as well as the formation of SOA from the photo-oxidation of SVOCs and IVOCs are described by the following reactions:



where i is the original volatility bin and $i - 1$ is the volatility bin with saturation concentration reduced by a factor of 10^2 . The term SOG corresponds to secondary organic gas that is produced by at least one chemical reaction in the atmosphere. The symbol “ \leftrightarrow ” denotes the equilibrium between the gas and the aerosol phases. It is worth mentioning that the production of RO_2 as an intermediate after the oxidation of SVOC and IVOC has been omitted since it would be essential only in cases where these reactions are a potentially significant sink of OH (i.e., in concentrated smoke plumes) (Alvarado et al., 2015). The model set up and the different aerosol types and chemical processes that are simulated by ORACLE for this study are illustrated in Fig. 1. More details about ORACLE can be found in Tsimpidi et al. (2014).

2.3 Emission inventory

The CMIP5 RCP4.5 emission inventory (Clarke et al., 2007) is used for the anthropogenic POA emissions from fossil fuel

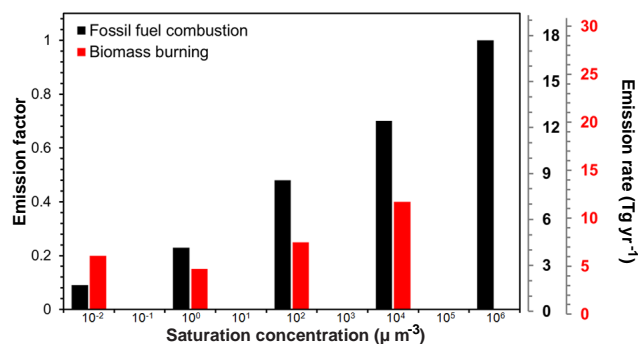


Figure 2. Volatility distribution for fuel combustion (in black) and biomass burning (in red) organic emissions. The emission factors for fuel combustion emissions are derived from Robinson et al. (2007) while for biomass burning POA emissions are from May et al. (2013) (shown in the primary y axis). The corresponding emission rates are also shown in the secondary y axis.

and biofuel combustion sources. The open biomass burning emissions from savanna burning and forest fires are based on the Global Fire Emissions Database (GFED v3.1; van der Werf et al., 2010). These emission data sets report the mass of the OC emitted. Therefore, in order to determine the total organic matter (OM) emitted (including any additional species associated with the carbon) OM/OC values of 1.3 for anthropogenic POA and 1.6 for open biomass burning POA are used. These values are based on the OM:OC ratios estimated by Canagaratna et al. (2015) for HOA and BBOA, respectively. Furthermore, the above emission data sets are monthly resolved and treat POA as non-reactive and non-volatile. However, only a fraction of this organic material is directly emitted in the aerosol phase as POA. Most of it is rapidly transferred to the gas phase where it can undergo chemical transformations and form SOA. Therefore, key input for the accurate description of these compounds and their chemical aging is the volatility distribution at 298 K. Figure 2 depicts the volatility distributions assumed for this study, which cover a range of 10^{-2} to $10^4 \mu\text{g m}^{-3}$ for open biomass burning (May et al., 2013) and 10^{-2} to $10^6 \mu\text{g m}^{-3}$ for fossil and biofuel combustion emissions (Robinson et al., 2007). Emission inventories are based on samples collected at aerosol concentrations up to $10^4 \mu\text{g m}^{-3}$ (Shrivastava et al., 2008; Robinson et al., 2010). As a result IVOC emissions with $C^* > 10^4 \mu\text{g m}^{-3}$ are missing from the traditional emission inventories and have to be accounted for by assigning additional emissions in this volatility range. We assume that the missing IVOC emissions from anthropogenic combustion are 1.5 times the traditional OA emissions included in the inventory (Shrivastava et al., 2008; Tsimpidi et al., 2010); therefore, the sum of the emission factors is 2.5. No additional IVOC emissions are assumed in the $C^* > 10^4 \mu\text{g m}^{-3}$ bins for open biomass burning and therefore the sum for the biomass burning emission factors is unity. As a result, 40 %

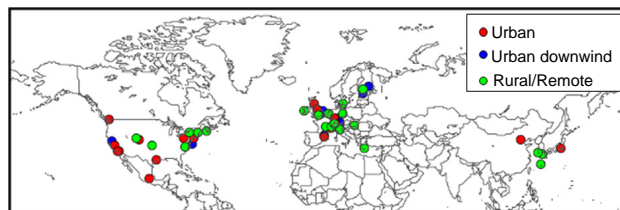


Figure 3. Location of the field measurement campaigns used for evaluating the model during 2001–2010. Urban, urban downwind and rural/remote areas are represented by red, blue, and green colors, respectively.

of the biomass burning OA emissions represents IVOCs with $C^* = 10^4 \mu\text{g m}^{-3}$ (Table 2). The sensitivity of our results to these assumptions will be discussed in a subsequent article in preparation. Overall, the decadal average global emission flux of SVOCs and IVOCs is 44 Tg yr^{-1} from anthropogenic combustion sources and 28 Tg yr^{-1} from open biomass burning sources.

3 Model evaluation methodology

3.1 Factor analysis of AMS measurements

During the period 2001–2010, 84 field campaigns were performed in the Northern Hemisphere using the AMS for measuring ambient OA concentrations in urban, urban-downwind, and rural environments (Fig. 3). Information for each of these campaigns is given in Tables S5–S7. The OA source apportionment for all sites was taken from the literature (Tables S5–S7) and performed using factor-analysis techniques classifying OA as HOA, corresponding to POA from fossil fuel combustion, and OOA, corresponding to SOA. Therefore, AMS HOA is compared with modeled fPOA, which is emitted and remains in the aerosol phase without undergoing chemical reactions, and AMS-OOA is compared with modeled SOA (the sum of SOA-sv, SOA-iv, and SOA-v), formed from the oxidation of gas-phase precursors (SVOCs, IVOCs, and VOCs). At many locations, PMF and other factor-analysis techniques identified two subtypes of OOA that differ in volatility and oxidation state: SV-OOA and LV-OOA. There are different potential interpretations of SV-OOA and LV-OOA. SV-OOA often correlates with semi-volatile species such as ammonium nitrate and is less oxygenated, consistent with relatively fresh SOA (Zhang et al., 2011; Ng et al., 2011). LV-OOA usually correlates with nonvolatile secondary species such as sulfate, and is highly oxygenated, consistent with regional aged OA (Zhang et al., 2011; Ng et al., 2011). Recently, Ehn et al. (2014) found a direct pathway, which leads to the formation of fresh LV-OOA from the oxidation of several biogenic VOCs. Here we test the hypothesis that SV-OOA corresponds to the first generation products and LV-OOA to the later generation ones.

Therefore, AMS SV-OOA is compared with the fraction of SOA-sv, SOA-iv, and SOA-v from the first oxidation step of SVOCs, IVOC, and VOCs as it is tracked separately (henceforth EMAC fresh SOA). Then AMS LV-OOA is compared with the fraction of SOA-sv, SOA-iv, and SOA-v from any additional oxidation step (henceforth EMAC aged SOA). Finally, in a few field campaigns, e.g., in the Alps (Lanz et al., 2010), residential wood burning was found to be a major source of OA. However, residential wood burning is included in EMAC as fPOA. To account for this inconsistency for the AMS data sets that include BBOA, we compare the sum of the simulated fPOA and bbPOA (henceforth EMAC POA) to the sum of the AMS HOA and BBOA (henceforth AMS POA). In data sets where OA from cooking activities has been resolved by the PMF analysis, AMS COA has not been taken into account for the model evaluation since these emissions are not included in our emission inventory.

3.2 Evaluation metrics

The mean bias (MB), mean absolute gross error (MAGE), normalized mean bias (NMB), normalized mean error (NME), and the root mean square error (RMSE) are used to assess the model performance:

$$\text{MAGE} = \frac{1}{N} \sum_{i=1}^N |P_i - O_i|, \quad (1)$$

$$\text{MB} = \frac{1}{N} \sum_{i=1}^N (P_i - O_i), \quad (2)$$

$$\text{NME} = \frac{\sum_{i=1}^N |P_i - O_i|}{\sum_{i=1}^N O_i}, \quad (3)$$

$$\text{NMB} = \frac{\sum_{i=1}^N (P_i - O_i)}{\sum_{i=1}^N O_i}, \quad (4)$$

$$\text{RMSE} = \left[\frac{1}{N} \sum_{i=1}^N (P_i - O_i)^2 \right]^{\frac{1}{2}}, \quad (5)$$

where O_i is the observed campaign average value of the i th OA component, P_i is the corresponding modeled value during the same period, and N is the total number of comparisons used for the evaluation. NME (in %) and MAGE (in $\mu\text{g m}^{-3}$) provide an estimate of the overall discrepancy between predictions and observations, while NMB (in %) and MB (in $\mu\text{g m}^{-3}$) are sensitive to systematic errors. RMSE (in $\mu\text{g m}^{-3}$) is the root of the mean square error, which incorporates both the variance of the prediction and its bias. Both NME and MAGE inherently include the corresponding bias, which is the reason why their magnitude is equal

or larger than NMB and MB, respectively. For an unbiased prediction, NME and MAGE express the variance. When NME and NMB or MAGE and MB are close, the discrepancy is explained as a systematic bias rather than scatter. When NME/MAGE exceeds NMB/MB, part of the discrepancy between predictions and observations is explained as scatter. To determine the effects of the site type, geographical location and the seasonal cycle on the model results, the evaluation metrics are calculated separately for urban, urban-downwind, and rural sites; European, North American, and Asian sites; and for four seasons (winter, spring, summer, and autumn).

4 Model results

4.1 OA from anthropogenic combustion

4.1.1 Geographical distribution

Figure 4 depicts the simulated, decadal average global surface concentrations of fPOA and fSOA from anthropogenic SVOC and IVOC sources (fossil and biofuel combustion). The average surface concentration of fPOA is $0.1 \mu\text{g m}^{-3}$. Higher fPOA concentrations (up to $14 \mu\text{g m}^{-3}$) are simulated over densely populated and highly industrialized areas (e.g., eastern China, northern India, central Europe) where there are substantial anthropogenic combustion emissions. Downwind of the sources fPOA concentrations decrease substantially since they are diluted and a large fraction is predicted to evaporate during transport. This results in a highly inhomogeneous spatial distribution of fPOA concentrations (Fig. 4a). In contrast, fSOA is more regionally distributed with high concentrations (up to $9.5 \mu\text{g m}^{-3}$) downwind of the anthropogenic sources due to its continuous production and long-range transport from SVOCs and IVOCs (Fig. 4b). This results in a continental fSOA background of $0.5\text{--}1 \mu\text{g m}^{-3}$ and in concentrations of around $1 \mu\text{g m}^{-3}$ over marine regions close to anthropogenic sources (e.g., Arabian Sea, Yellow Sea). The average surface concentration of fSOA is $0.26 \mu\text{g m}^{-3}$ with 73 % of it originating from the oxidation of IVOC emissions. This result supports the hypothesis of several recent studies that IVOC emission and oxidation may be a significant SOA source that has been missing from chemistry climate models (Jathar et al., 2011; Tsimpidi et al., 2014). The relatively small contribution (25 %) of SVOCs to total fSOA follows from its low emissions compared to the IVOCs (2 times lower) and by the fact that a significant fraction of SVOCs stays in the aerosol phase (as POA) without undergoing chemical reactions (Tsimpidi et al., 2014).

The fraction of fossil and biofuel combustion OA (fOA) that is formed through the oxidation of gas-phase species, fSOA/fOA, is consistently high with values ranging from around 20 % close to the sources to 100 % away in remote regions with a global average of 83 % at the surface (Fig. 5a). This suggests that over urban areas both fPOA and fSOA

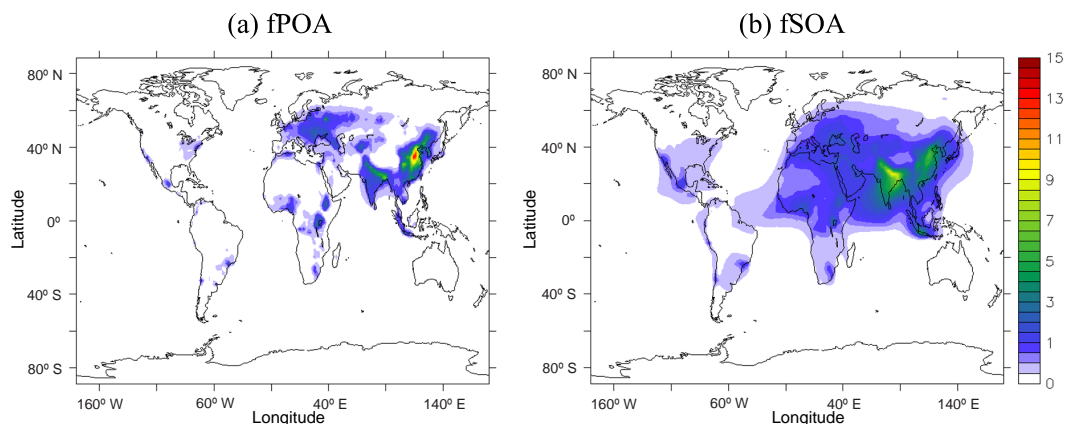


Figure 4. Predicted average surface concentrations (in $\mu\text{g m}^{-3}$) of (a) POA from fuel combustion sources (fPOA) and (b) SOA from the oxidation of SVOCs and IVOCs from fuel combustion sources (fSOA) during the years 2001–2010.

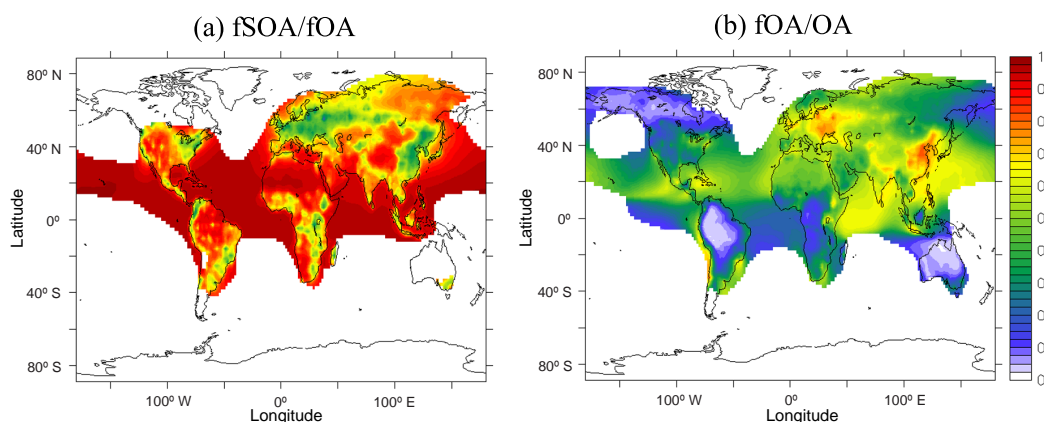


Figure 5. Predicted ratio of (a) fuel combustion SOA (fSOA) to total fuel combustion OA (sum of fPOA and fSOA) and (b) fuel combustion OA to total OA (sum of fOA, bbOA, aSOA, and bSOA) during the years 2001–2010.

contribute significantly to the overall OA mass, whereas further downwind and in rural areas SOA formation dominates since POA decreases substantially due to dilution and evaporation. The OA due to anthropogenic combustion sources contributes significantly to total OA over the continents in the Northern Hemisphere (Fig. 5b). The highest contribution is predicted over eastern China (83 %) and the lowest over the southeastern USA (23 %). Over mid-latitude oceans, the contribution of fOA to total OA is also high (around 60 %) due to the long-range transport of SOA. On the other hand, fOA/OA is very low (0–10 %) over the tropical and boreal forest regions in contrast to the significant bbOA and bSOA-v concentrations over these areas. The eastern part of the Eurasian boreal forest is an exception since the lower emissions of bbOA together with the considerable amount of fSOA transported from Europe results in fOA/OA fractions of about 40 %. Overall, the predicted global average fOA/OA is 38 %. This result highlights the importance of anthropogenic emissions for global OA levels, also suggested by other recent

studies (Carslaw et al., 2013; Lee et al., 2013; Spracklen et al., 2011).

4.1.2 Temporal profile

Table 1 shows the decadal average tropospheric burden of fPOA and fSOA. The decadal average tropospheric burden of total fOA is 0.63 Tg (10 % fPOA and 90 % fSOA). The tropospheric fSOA/fOA is higher than at the surface since SVOC and IVOC continue forming fSOA at higher altitudes (Tsimpidi et al., 2014).

The wintertime burden of fPOA is 36 % higher than its annual average value (Fig. 6a). This increase is partially driven by the seasonality of the emissions since anthropogenic OA emissions are 12 % higher during winter compared to the annual average. Furthermore, the lower temperatures that occur during winter in the Northern Hemisphere drive the gas-particle partitioning of freshly emitted SVOCs to the aerosol phase resulting in higher fPOA concentrations. At the same

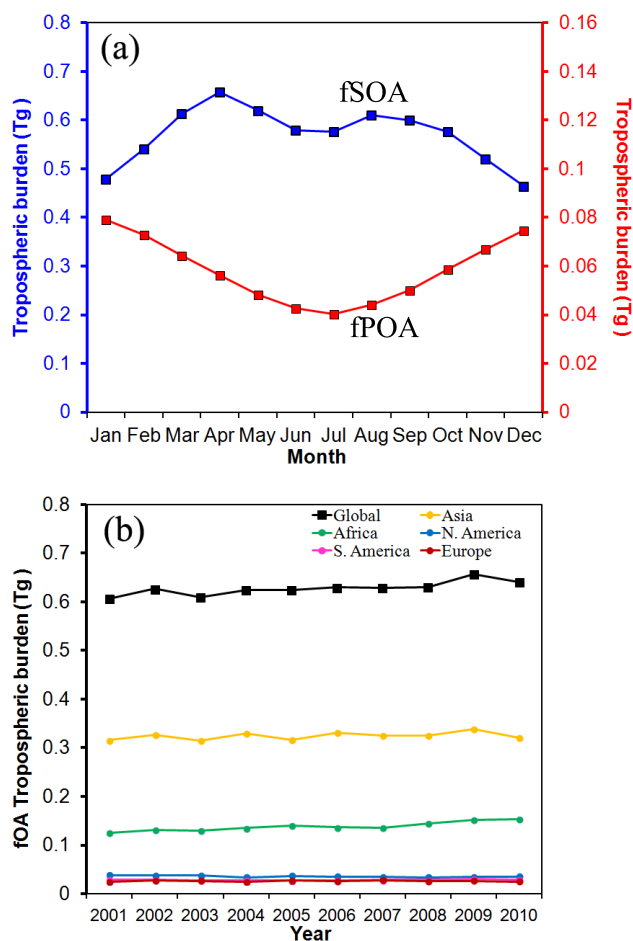


Figure 6. (a) Average predicted tropospheric burden (Tg) of fSOA (in blue, primary y axis) and fPOA (in red, secondary y axis) and (b) annually averaged tropospheric burden of total fuel combustion OA (fOA) during 2001–2010.

time, fewer SVOCs are available in the gas phase to react with the lower wintertime OH resulting in reduced formation of fSOA. The wintertime tropospheric burden of fSOA is 16 % lower than the annual average value (Fig. 6a) representing 87 % of the fOA. During summer, the photo-oxidation of SVOC and IVOC is significantly enhanced; however, the increase in fSOA mass is compensated by evaporation due to the high temperatures resulting in an overall increase of only 3 % compared to the annual average values. High temperatures during summer also result in a significant decrease of fPOA due to evaporation, i.e., a 27 % decrease compared to the annual average tropospheric burden (Fig. 6a). Overall, the tropospheric fSOA : fOA during summer increases to 93 %. The highest fSOA concentrations are predicted during spring (i.e., April) when photochemistry is active and the moderately low temperatures favor the partitioning into the aerosol phase (Fig. 6a).

Figure 6b depicts the annual tropospheric fOA variability over the simulated years (2001 to 2010). The variability of

Table 1. Predicted tropospheric burden in Tg of organic aerosol components during the decade 2001–2010.

OA component	Tropospheric burden (Tg)	Monthly standard deviation (σ)
fPOA	0.06	0.01
fSOA	0.57	0.06
bbPOA	0.18	0.13
bbSOA	0.42	0.27
aSOA	0.44	0.08
bSOA	0.31	0.10
OA	1.98	0.54

the model predicted fOA is very low (± 4 %) since anthropogenic emissions are assumed to have small differences between the simulated years (Clarke et al., 2007). The anthropogenic OC emissions from fossil and biofuel combustion increase by $1.23 \text{ Tg C yr}^{-1}$ (10 %) during the simulated decade. Over Asia and Africa, anthropogenic OC emissions have increased by 12 and 33 %, respectively, during the simulated decade. On the other hand, anthropogenic OC emissions over North America have decreased by 15 % during the same period. Over South America, anthropogenic OC emissions have decreased up to the year 2005 (10 %) and then remained about constant until the end of the decade. Over Europe, anthropogenic OC emissions have increased up to the year 2005 (5 %) and then started to decrease reaching 4 % lower emissions (compared to 2001) by the end of the decade. However, the simulated fOA tropospheric burdens over the continents (Fig. 6b) do not reflect this clear trend of emissions since other factors (i.e., meteorology) play an important role. Overall, the lowest fOA global tropospheric burden is calculated during the years 2001 and 2003 (0.61 Tg yr^{-1}) and the highest during the year 2009 (0.66 Tg yr^{-1}).

4.2 OA from open biomass burning

4.2.1 Geographical distribution

Figure 7 depicts the simulated decadal average global surface concentrations of bbPOA and bbSOA. The average surface concentration of bbPOA is $0.11 \mu\text{g m}^{-3}$. The highest bbPOA concentrations (up to $7.7 \mu\text{g m}^{-3}$) are predicted over the tropical rainforests (i.e., Amazon, Congo, and Southeast Asia) and the boreal forests (i.e., Alaska, Canada, and Russia) due to substantial emissions from forest and savannah fires. Similar to fPOA, bbPOA levels rapidly decrease as the air masses travel from the sources due to dilution and evaporation (Fig. 7a). The average surface concentration of bbSOA is $0.15 \mu\text{g m}^{-3}$. In contrast to anthropogenic combustion emissions, IVOCs are assumed to account for only 40 % of the total open biomass burning emissions. Nevertheless, the model

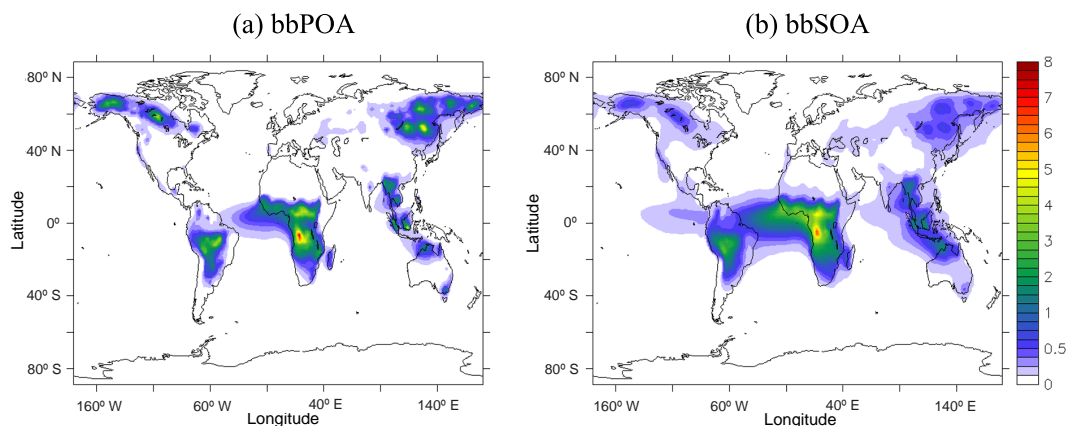


Figure 7. Predicted average surface concentrations (in $\mu\text{g m}^{-3}$) of (a) POA from biomass burning sources (bbPOA) and (b) SOA from the oxidation of SVOCs and IVOCs from biomass burning sources (bbSOA) during the years 2001–2010.

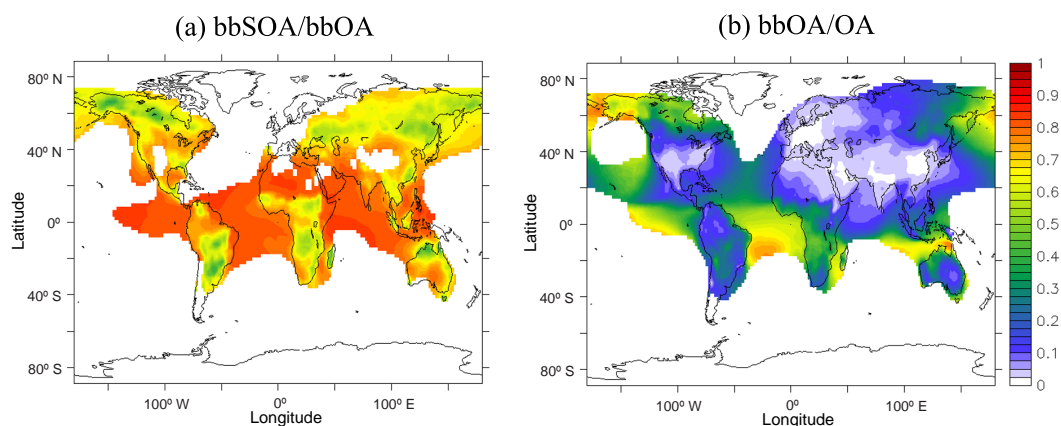


Figure 8. Predicted ratio of (a) biomass burning SOA (bbSOA) to total biomass burning OA (sum of bbPOA and bbSOA) and (b) biomass burning OA to total OA (sum of fOA, bbOA, aSOA, and bSOA) during the years 2001–2010.

predicts that the bbSOA formed due to the oxidation of IVOCs (46 %) is similar to that from the oxidation of SVOCs (54 %). This result corroborates our finding that IVOCs are a significant source of SOA. bbSOA concentrations are more spatially homogeneous compared to bbPOA reaching high levels (up to $6.4 \mu\text{g m}^{-3}$) over a wide area covering most of South America, central and southern Africa, and Southeast Asia, including Indonesia (Fig. 7b). The atmosphere over the South Atlantic Ocean is also strongly influenced by the long-range transport of bbSOA from the Congo Basin ($1\text{--}3 \mu\text{g m}^{-3}$). Over these areas, the atmospheric conditions are favorable for the photochemical oxidation of SVOCs and IVOCs. On the other hand, over the boreal forests, the low temperatures favor the partitioning of SVOCs into the particulate phase forming bbPOA, and at the same time the photo-oxidation of IVOCs is slow. This results in moderate average bbSOA concentrations around $0.5 \mu\text{g m}^{-3}$.

Figure 8a depicts the predicted decadal average contribution of bbSOA to total bbOA (bbSOA/bbOA) at the surface.

bbSOA/bbOA is high with values ranging from around 35 % over the tropical and boreal forests to 85 % in areas downwind and over the oceans. The global average bbSOA/bbOA at the surface is predicted to be 72 %. This result indicates that even though the biomass burning emissions are distributed in relatively low-volatility bins ($C^* \leq 10^4 \mu\text{g m}^{-3}$), bbSOA still exceeds primary biomass burning OA on a global scale. Figure 8b depicts the decadal average surface contribution of bbOA to total OA (bbOA/OA). As expected, bbOA contributes significantly to total OA over the tropical and boreal forests (around 60 %) while it has a smaller impact on OA levels over the mid-latitude continents of the Northern Hemisphere. This result does not include other types of biomass combustion (e.g., for residential heating) that often contribute significantly in urban areas (Chen et al., 2007; Wang et al., 2007; Lanz et al., 2010). High bbOA contributions are also predicted downwind of the boreal forests (up to 80 %). Furthermore, the bbOA/OA ratio is high (50–90 %) off the west coast of Africa, South America, and Indonesia.

These high values are due to the chemical aging of biomass burning SVOCs and IVOCs in contrast to the chemical products of biogenic VOCs, which are not allowed to participate in additional photochemical reactions (Tsimpidi et al., 2014). Overall, the global average bbOA/OA is predicted to be 26 %.

4.2.2 Temporal evolution

The decadal average tropospheric burden of total bbOA is 0.59 Tg yr^{-1} (30 % bbPOA, 70 % bbSOA) (Table 1). The fraction of bbOA that is secondary is less than that of fOA (90 %).

The interannual variability of bbPOA and bbSOA is high due to the seasonality of fires (Fig. 9a). During July to September (dry season) intense wildfires are reported over the tropics related to the low precipitation and high temperatures. This results in high biomass burning emissions, which together with the intense photochemical activity result in bbOA tropospheric burdens of up to 1.4 Tg yr^{-1} during August (130 % higher than the annual average). The lowest bbOA tropospheric burdens are estimated during the wet season (0.21 Tg yr^{-1} during April, 64 % lower than the annual average). Furthermore, during the dry season OA consists mainly of bbOA over the tropical rainforests due to the intense wildfires, whereas during the wet season OA consists mainly of biogenic SOA since biomass burning emissions are low. As a result, the bbOA/OA has a significant seasonal variability as well; during the dry season the global average bbOA/OA increases significantly (e.g., 41 % during August; not shown) while during the wet season it is significantly lower (e.g., 11 % during March; not shown).

The decadal variability of the model predictions is also important since open biomass burning emissions can vary significantly from year to year (Fig. 9b). The years 2001 and 2009 had relatively low fire activity ($13.5 \text{ Tg C yr}^{-1}$) and the bbOA annual tropospheric burden was 0.47 Tg yr^{-1} (21 % lower than the decadal average). During these 2 years tropospheric bbOA was lower over both the Amazon and the Congo basins (Fig. 9b). The year of 2010 on the other hand was characterized by severe wildfires, especially in the Amazon region (OC emissions were twice the decadal average) resulting in a global bbOA source of 0.72 Tg yr^{-1} (21 % higher than the decadal average). Over the Congo Basin, the calculated tropospheric burden peaks during the years 2005 and 2010 (Fig. 9b), whereas over the Amazon Basin the highest burdens are calculated during the years 2007 and 2010. The above results are consistent with Chen et al. (2013), who analyzed satellite data to detect the fire activity over the Amazon rainforest and reported a 2-fold increase in fire activity during 2010 compared to 2009.

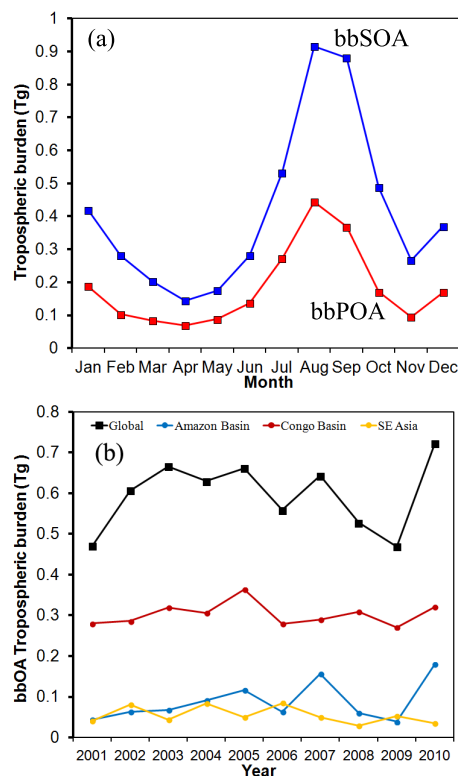


Figure 9. (a) Monthly averaged predicted tropospheric burden (Tg) of bbSOA (in blue) and bbPOA (in red) and (b) annual average tropospheric burden of total biomass burning OA (bbOA) during 2001–2010.

5 Comparison with AMS data

5.1 Evaluation over urban areas

The spatial resolution used in the current application as well as in most global model applications (Tsigaridis et al., 2014) can introduce potentially significant errors over urban areas. Other issues can also add to the model–measurement discrepancy over cities. For example, global models, including EMAC, lack OA emissions from residential and commercial cooking activities (Tsigaridis et al., 2014). However, cooking can be an important source of OA that can contribute significantly to measured POA (around 50 %) and total OA (15–20 %) over urban areas (Sun et al., 2011; Mohr et al., 2012; Ge et al., 2012; Hayes et al., 2013). Therefore, our analysis and use of the corresponding urban AMS data sets should be viewed as an effort to quantify the magnitude of these errors. In addition, there have been a number of recent studies using global atmospheric chemistry models to investigate the link between premature mortality and atmospheric aerosols in urban and rural environments (Lelieveld et al., 2015). Evaluating global models over urban locations can provide useful information about their potential biases in these locations.

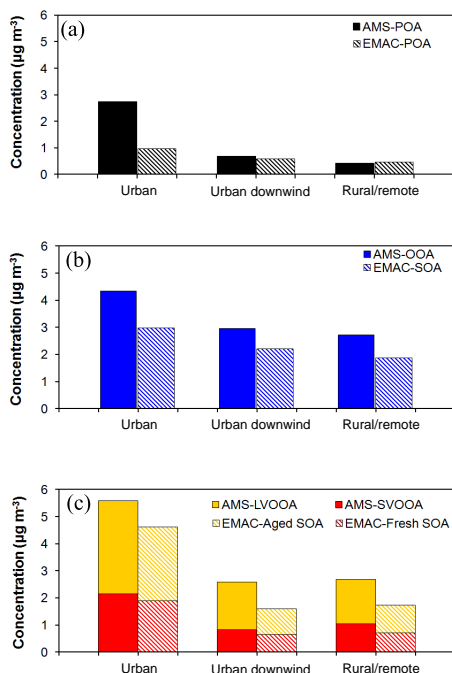


Figure 10. Comparison of average (a) EMAC predicted POA (sum of fPOA and bbPOA) to AMS-POA (sum of AMS-HOA and AMS-BBOA), (b) EMAC predicted SOA to AMS-OOA, and (c) EMAC predicted fresh and aged SOA to AMS-SVOOA and AMS-LVOOA from 84 data sets over urban, urban downwind, and rural/remote areas during 2001–2010.

AMS observations indicate that over urban areas the POA (sum of HOA and BBOA) concentration is relatively high, whereas further downwind and in rural areas it decreases substantially due to dilution and evaporation (Fig. 10a). The model is able to reproduce this trend; however, it significantly underpredicts ($\text{NMB} = -65\%$, Table 2) the high values of POA over urban areas and especially over densely populated areas such as Beijing, Tokyo and Mexico City (Table S5; Fig. 11a). This underprediction appears to be typical for global models (Tsigaridis et al., 2014) and is partly associated with the limited spatial resolution of the model (the size of a grid cell used typically exceeds the size of most urban centers) and the lack of COA emissions. The model underestimates SOA ($\text{NMB} = -33\%$, Table 2) over densely populated areas such as Beijing and Mexico City (Table S5; Fig. 12a) partially due to its limited spatial resolution. In addition, the lack of COA emissions can be considered as a possible cause of OOA underestimation by the model over urban and urban-downwind areas (see below) given that COA can be oxidized and form SOA over the urban center and further downwind. Overall, the underestimation of OA over urban locations indicates that global exposure studies (Lelieveld et al., 2015) provide a lower limit of the actual contribution of OA to premature mortality over large urban areas.

Given that the model cannot sufficiently reproduce the concentrations of POA and SOA over urban locations, AMS data from these locations is not included for the seasonal, continental, and total (annual) evaluation of the model presented below. Especially for the seasonal model evaluation, most of the urban field campaigns were conducted either during winter or summer. Therefore, including these locations in our analysis is expected to bias the model performance during winter and summer leading to a potential misinterpretation of the corresponding seasonal results.

5.2 Spatial evaluation

5.2.1 POA

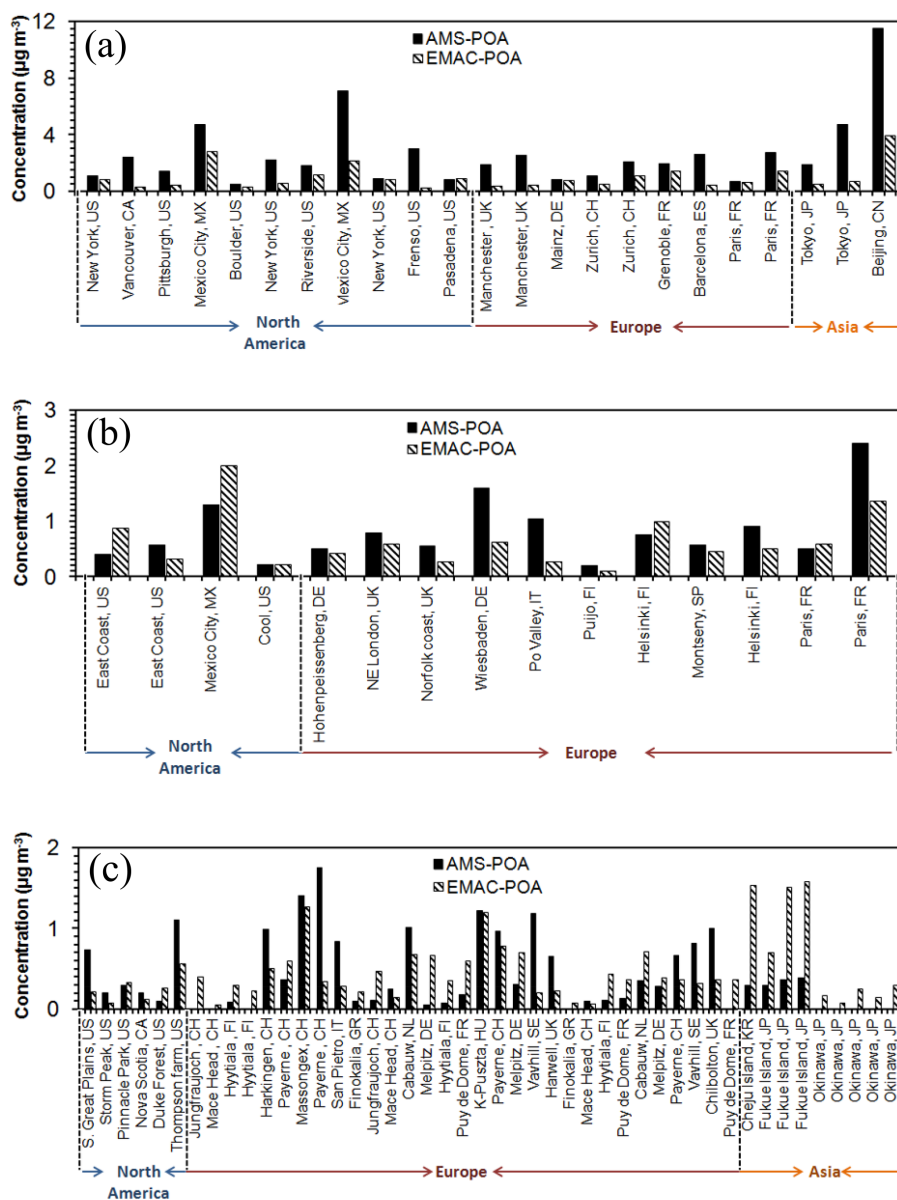
Over urban-downwind locations, the model does a better job than urban locations in reproducing the measured POA values (Table 3). This can be verified by focusing on specific field campaigns that provide data from both the urban center and urban-downwind locations over the same period of time (i.e., MILAGRO over Mexico City and MEGAPOLI over Paris). Over these areas the model captures the measured POA concentrations downwind of the urban center (Table S6; Fig. 11b) but it significantly underpredicts the POA concentrations measured in the urban center (Table S5; Fig. 11a). Overall, in urban-downwind and rural areas the model captures the lower POA levels (Figs. 10a and 11). Over urban-downwind areas, the model slightly underpredicts POA ($\text{NMB} = -15\%$) while over rural areas it overpredicts by $0.04 \mu\text{g m}^{-3}$ (Table 3). However, over rural areas with high BBOA concentrations (e.g., Massognex, Payerne) the model underpredicts POA (Table S7; Fig. 11c) indicating that biomass burning and/or biofuel use in residential areas may be underestimated in the emission inventory.

In Europe, the model underestimates POA concentrations ($\text{NMB} = -23\%$; Table 3). However, the comparison of simulated fPOA with AMS HOA (i.e., excluding BBOA from the comparison) suggests that the model overpredicts POA over Europe with a $\text{NMB} = 20\%$ (not shown). This result underscores the underestimated emissions from residential biofuel use as a prominent cause of the model bias over Europe. The possible underestimation of biomass/biofuel burning emissions in European residential areas has also been reported by other studies (Bergström et al., 2012; Kostenidou et al., 2013; Denier van der Gon et al., 2016). Over North America, the model reproduces well the measured HOA (Table 3). Over Asia, the model overestimates the low values of POA measured by AMS (Table 3) mainly due to the high simulated bbPOA concentrations (45% of total POA) transported from the boreal forests of northeast Asia.

Table 2. Statistical evaluation of EMAC results against AMS measurements over urban locations of the Northern Hemisphere during 2001–2010.

EMAC element	AMS element	Number of data sets	Mean observed ($\mu\text{g m}^{-3}$)	Mean predicted ($\mu\text{g m}^{-3}$)	MAGE ($\mu\text{g m}^{-3}$)	MB ($\mu\text{g m}^{-3}$)	NME (%)	NMB (%)	RMSE ($\mu\text{g m}^{-3}$)
POA*	HOA + BBOA	23	2.70	0.98	1.73	−1.72	64	−64	2.58
SOA	OOA	23	4.25	2.85	1.97	−1.40	46	−33	2.50
Aged SOA	LV-OOA	10	3.43	2.72	1.47	−0.72	43	−21	2.04
Fresh SOA	SV-OOA	10	2.14	1.88	0.69	−0.26	32	−12	0.81

* Sum of fPOA and bbPOA.

**Figure 11.** Comparison of EMAC POA (sum of fPOA and bbPOA) to AMS POA (sum of HOA and BBOA) from 84 data sets worldwide over (a) urban, (b) urban downwind, and (c) rural/remote areas during 2001–2010.

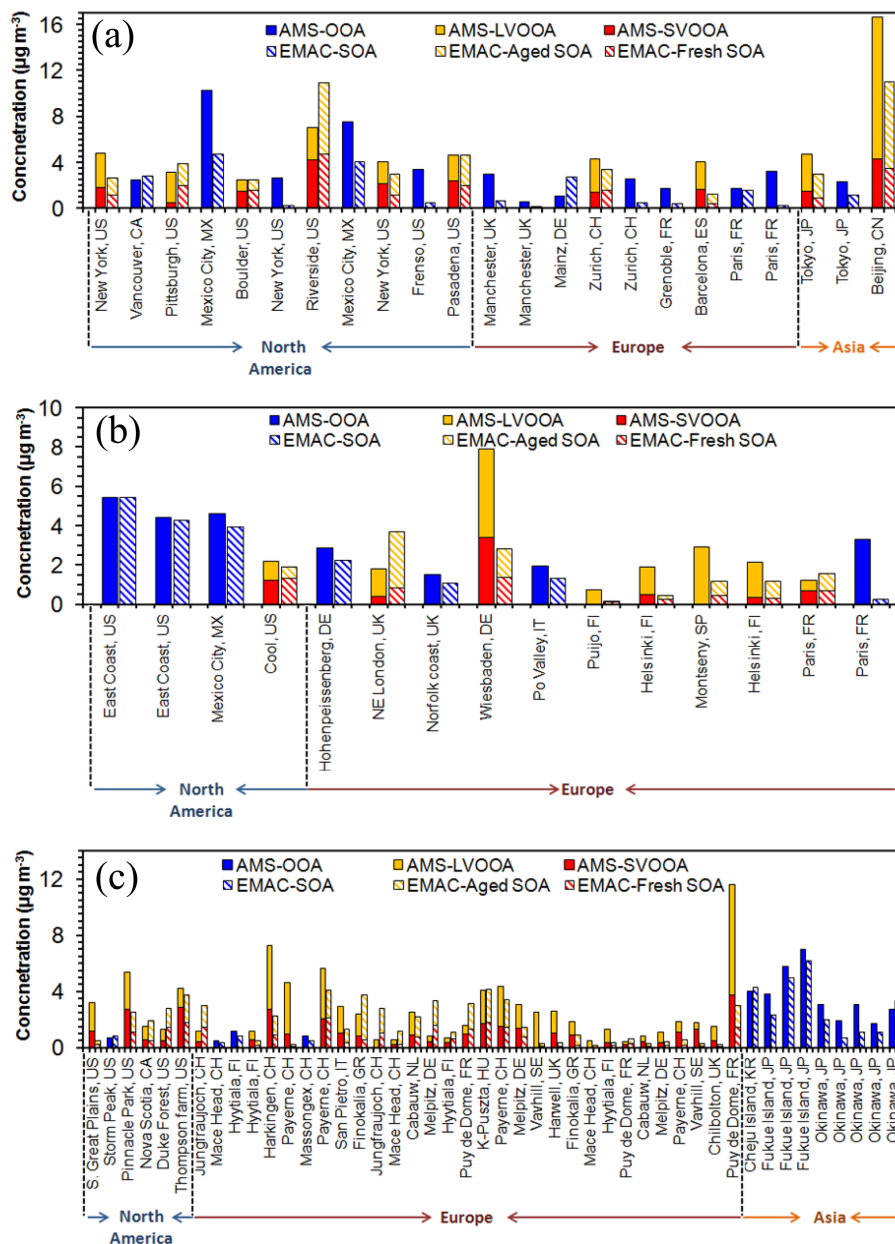


Figure 12. Comparison of EMAC SOA (fresh SOA and aged SOA) to AMS OOA (SV-OOA and LV-OOA) from 84 data sets worldwide over (a) urban, (b) urban downwind, and (c) rural/remote areas during 2001–2010.

5.2.2 SOA

Both AMS and EMAC model results indicate that SOA (and OOA) is high over all environments considered (Table 4). The highest concentrations are found over urban locations ($\text{AMS-OOA} = 4.33 \mu\text{g m}^{-3}$ and $\text{EMAC-SOA} = 2.97 \mu\text{g m}^{-3}$) while further downwind SOA concentrations decrease by 37% over rural locations according to both AMS and EMAC results (Fig. 10b). This indicates that the initial emissions of VOCs, IVOCs, and SVOCs are photo-oxidized rapidly in the urban environment producing SOA,

while their atmospheric aging and further production of SOA is offset by dilution as the air masses travel from the urban centers. EMAC does a reasonable job in reproducing SOA concentrations (Table 4); however, a systematic under-prediction is found in all types of environments. The best model performance is achieved over urban downwind locations ($\text{NMB} = -25\%$) followed by urban and rural areas ($\text{NMB} = -31$ and -32% , respectively). The model significantly underpredicts SOA over specific urban-downwind and rural areas. In most of these cases the field campaign was short (up to 1 week) and the results were subject to specific

Table 3. Statistical evaluation of EMAC POA (sum of fPOA and bbPOA) against AMS POA (sum of HOA and BBOA) in the Northern Hemisphere during 2001–2010.

Site type ^a	Number of data sets	Mean observed ($\mu\text{g m}^{-3}$)	Mean predicted ($\mu\text{g m}^{-3}$)	MAGE ($\mu\text{g m}^{-3}$)	MB ($\mu\text{g m}^{-3}$)	NME (%)	NMB (%)	RMSE ($\mu\text{g m}^{-3}$)
Urban downwind	15	0.82	0.64	0.38	−0.18	47	−22	0.50
Rural/remote	46	0.43	0.47	0.37	0.04	87	9	0.5
Continent ^b								
Europe	42	0.61	0.47	0.36	−0.14	59	−23	0.47
N. America	10	0.51	0.50	0.29	−0.01	57	−3	0.37
Asia	9	0.15	0.69	0.54	0.54	363	363	0.72
Season ^c								
Winter	6	1.18	0.74	0.60	−0.44	51	−37	0.76
Spring	30	0.42	0.53	0.41	0.11	97	26	0.52
Summer	14	0.50	0.44	0.30	−0.06	59	−13	0.39
Autumn	11	0.49	0.42	0.27	−0.07	54	−15	0.37
Total	61	0.53	0.51	0.38	−0.02	71	−3	0.50

^a Statistics are calculated for a specific site type during all seasons. ^b Statistics are calculated for a specific continent excluding the values from urban areas. ^c Statistics are calculated for a specific season excluding the values from urban areas.

Table 4. Statistical evaluation of EMAC SOA against AMS OOA in the Northern Hemisphere during 2001–2010.

Site type ^a	Number of data sets	Mean observed ($\mu\text{g m}^{-3}$)	Mean predicted ($\mu\text{g m}^{-3}$)	MAGE ($\mu\text{g m}^{-3}$)	MB ($\mu\text{g m}^{-3}$)	NME (%)	NMB (%)	RMSE ($\mu\text{g m}^{-3}$)
Urban downwind	15	2.98	2.07	1.20	−0.91	40	−30	1.77
Rural/remote	46	2.72	1.86	1.45	−0.86	54	−32	2.09
Continent ^b								
Europe	42	2.47	1.49	1.59	−0.98	64	−39	2.28
N. America	10	3.29	2.78	0.91	−0.51	28	−15	1.37
Asia	9	3.68	2.89	1.00	−0.79	27	−22	1.11
Season ^c								
Winter	6	2.81	0.50	2.31	−2.31	82	−82	2.65
Spring	30	2.22	1.79	0.97	−0.43	44	−20	1.18
Summer	14	4.30	2.89	2.04	−1.41	47	−33	3.20
Autumn	11	2.35	1.78	1.22	−0.57	52	−25	1.39
Total	61	2.78	1.91	1.39	−0.87	50	−31	2.02

^a Statistics are calculated for a specific site type during all four seasons. ^b Statistics are calculated for a specific continent excluding the values from urban areas. ^c Statistics are calculated for a specific season excluding the values from urban areas.

pollution episodes, which cannot be captured by our model (e.g., Puy de Dome, Table S7; Fig. 12c).

Over the continents, the largest SOA underestimation is found over Europe (NMB = −39%). Similar to POA, it is mostly driven by the model underperformance over sites with high biomass burning sources and biofuel use (e.g., Harkingen and Payern, CH; Fig. 12). Over North America, the model simulates well the SOA formation with

NMB = −15%. Isoprene epoxydiols-derived secondary organic aerosol (IEPOX-SOA), a type of SOA likely formed via processing of later generation isoprene products in aqueous acidic aerosols, has been recently suggested as an important source of SOA close to isoprene emissions (Hu et al., 2015). The model does not simulate SOA formation from aqueous-phase reactions and therefore does not produce IEPOX-SOA, which may lead to an underestimation of SOA

over some sites in North America that are strongly influenced by isoprene emissions (e.g., over the Pinnacle state park, NY; Table S7; Fig. 12c). Over Asia, the model slightly underestimates SOA with NMB = -22 % (Table 4; Fig. 12).

In most of the available data sets (41 out of 84), PMF provides information for the two subtypes of OOA (LV-OOA and SV-OOA). Both PMF and EMAC results indicate that aged SOA (or LV-OOA) is higher than fresh SOA (or SV-OOA) regardless of the type of environment (Tables 5 and 6). However, in North America, AMS SV-OOA is slightly higher than LV-OOA while EMAC calculations indicate the opposite (Tables 5 and 6). Despite this discrepancy, the model reproduces well both the fresh SOA (NMB = -29 %) and aged SOA (NMB = -20 %) over North America while over Europe the underestimation is larger (Tables 5 and 6). The EMAC performance is better over urban locations where it reproduces the high levels of aged SOA with NMB = -21 % and NME = 43 % (Table 2). Over urban-downwind and rural locations EMAC underpredicts aged SOA with NMB = -47 and -38 %, respectively (Table 5). The performance of the model for fresh SOA is better compared to aged SOA (Table 5), with the exception of North America, indicating that the modeled OA aging parameterization may underestimate the SOA produced from chemical reactions during transport and requires improvements. Similar to aged SOA, the best performance of the model for fresh SOA is obtained over urban locations (NMB = -12 %).

5.3 Seasonal evaluation

5.3.1 POA

The model performs best during summer (RMSE = 0.4, NMB = -3 %), followed by autumn (RMSE = 0.37, NMB = -15 %) and spring (RMSE = 0.52, NMB = 21 %). During winter EMAC underpredicts POA with NMB = -34 % (Table 3; Fig. 13a). This result corroborates our hypothesis that residential biofuel emissions may be underestimated in the inventory since residential heating is expected during winter. Furthermore, since vehicle catalysts require a certain temperature to work to full efficiency, emissions from gasoline and diesel engines are significantly higher during the warm-up phase of the car (Westerholm et al., 1996). Typically, the additional emissions during the warm-up phase (or cold-start emissions) are not accounted for in emission inventories, which are based on measurements at an ambient temperature of 23 °C (Weilenmann et al., 2009). However, cold-start emissions increase considerably at lower ambient temperatures varying by more than 1 order of magnitude between 23 and -20 °C (Weilenmann et al., 2009), and thus significant underestimations of OA emissions from the transport sector can be expected during wintertime. Kopacz et al. (2010) provided a global estimate of CO sources by adjoint inversion of satellite data sets and reported an underestimation of CO sources during the

winter season due to larger than expected CO emissions from vehicle cold starts and residential heating. Errors in the POA volatility distributions can also explain parts of the model-measurement discrepancy. An overestimation of the fresh POA volatility will favor its evaporation resulting in an underestimation of POA levels by the model. Another source of the POA underestimation by EMAC may be the treatment of wet deposition. The sensitivity of the results to the emission and deposition parameterizations (e.g., the Henry's law constants for the organic vapors) will be tested in a subsequent article in preparation.

According to recent studies (Cappa and Wilson, 2012; Aumont et al., 2012; Zhang et al., 2013), not all oxidation products of SVOCs and IVOCs can be assigned to the OOA mass fraction since they are not sufficiently oxidized. Fountoukis et al. (2014) assumed that 50 % of the simulated SOA-sv and SOA-iv is still considered as HOA by the AMS analysis and found significant improvements in view of the modeled bias for POA. In this study we tested this hypothesis and we considered POA to be the sum of fPOA and bbPOA and 50 % of the SOA-sv and SOA-iv produced from the first oxidation step of SVOCs and IVOCs, respectively. We assumed that SOA-sv and SOA-iv produced during subsequent oxidation steps together with all the SOA-v are sufficiently oxidized to be considered 100 % OOA. Following this hypothesis the model performance improved during winter (NME = 55 % $\mu\text{g m}^{-3}$ and NMB = -28 %) and autumn (NME = 50 % $\mu\text{g m}^{-3}$ and NMB = 1 %) and deteriorated during spring (NME = 110 % $\mu\text{g m}^{-3}$ and NMB = 49 %) and summer (NME = 71 % $\mu\text{g m}^{-3}$ and NMB = 16 %) when the oxidation of SVOCs and IVOCs is enhanced significantly.

5.3.2 SOA

The best performance of the model is found for spring (NME = 46 %, NMB = -24 %) followed by the autumn (NME = 52 %, NMB = -25 %) and summer (NME = 44 %, NMB = -28 %) (Table 4; Fig. 13b). However, during winter the model strongly underpredicts OOA concentrations (NME = 80 %, NMB = -80 %). The overall underprediction of OOA concentrations indicates that the model is missing an important source or formation pathway of SOA. Possible underestimation of residential biofuel emissions in our model, identified during the spatial and seasonal evaluation of simulated POA, can lead to an underestimation of SOA formed from the oxidation of these emissions during winter. Fountoukis et al. (2016) also reported low modeled SOA values compared to AMS OOA over the Paris region and attributed this discrepancy to the transformation of BBOA to OOA without the presence of sunlight reported by some recent studies (Bougiatioti et al., 2014; Crippa et al., 2013b). Underestimation of cold-start vehicle emissions during winter can also lead to a significant underestimation of SOA, since SOA produced from organic compounds emitted during the warm-up phase can be 3–7 times higher than SOA produced

Table 5. Statistical evaluation of EMAC aged SOA against AMS LV-OOA in the Northern Hemisphere during 2001–2010.

Site type ^a	Number of data sets	Mean observed ($\mu\text{g m}^{-3}$)	Mean predicted ($\mu\text{g m}^{-3}$)	MAGE ($\mu\text{g m}^{-3}$)	MB ($\mu\text{g m}^{-3}$)	NME (%)	NMB (%)	RMSE ($\mu\text{g m}^{-3}$)
Urban downwind	8	1.77	0.94	1.28	−0.83	72	−47	1.55
Rural/remote	33	1.65	1.02	1.17	−0.63	71	−38	1.69
Continent ^b								
Europe	35	1.71	0.98	1.24	−0.73	73	−43	0.47
N. America	6	1.45	1.17	0.87	−0.28	60	−20	1.00
Asia	–	–	–	–	–	–	–	–
Season ^c								
Winter	3	2.36	0.20	2.16	−2.16	91	−91	2.36
Spring	18	1.06	0.81	0.82	−0.25	77	−24	1.03
Summer	11	2.64	1.55	1.79	−1.09	68	−41	2.47
Autumn	9	1.49	1.01	0.89	−0.48	59	−32	1.10
Total	41	1.68	1.01	1.19	−0.67	71	−40	1.67

^a Statistics are calculated for a specific site type during all four seasons. ^b Statistics are calculated for a specific continent excluding the values from urban areas. ^c Statistics are calculated for a specific season excluding the values from urban areas.

Table 6. Statistical evaluation of EMAC fresh SOA against AMS SV-OOA in the Northern Hemisphere during 2001–2010.

Site type ^a	Number of data sets	Mean observed ($\mu\text{g m}^{-3}$)	Mean predicted ($\mu\text{g m}^{-3}$)	MAGE ($\mu\text{g m}^{-3}$)	MB ($\mu\text{g m}^{-3}$)	NME (%)	NMB (%)	RMSE ($\mu\text{g m}^{-3}$)
Urban downwind	8	0.81	0.64	0.41	−0.17	51	−21	0.76
Rural/remote	33	1.03	0.70	0.64	−0.33	62	−32	0.85
Continent ^b								
Europe	35	0.90	0.63	0.56	−0.27	62	−30	0.81
N. America	6	1.51	1.07	0.80	−0.44	53	−29	0.96
Asia	–	–	–	–	–	–	–	–
Season ^c								
Winter	3	0.87	0.18	0.69	−0.69	79	−79	0.76
Spring	18	0.54	0.37	0.46	−0.17	86	−31	0.60
Summer	11	1.89	1.22	0.96	−0.67	51	−36	1.27
Autumn	9	0.83	0.86	0.39	0.03	47	4	0.52
Total	41	0.99	0.69	0.60	−0.30	60	−30	0.83

^a Statistics are calculated for a specific site type during all four seasons. ^b Statistics are calculated for a specific continent excluding the values from urban areas. ^c Statistics are calculated for a specific season excluding the values from urban areas.

when the catalyst is hot (Gordon et al., 2014). Furthermore, ORACLE assumes that the only source of SOA is the homogeneous gas-phase photochemical oxidation of SOA precursors. Therefore, the negative bias of the model during winter may also be explained by its inability to simulate SOA formed from aqueous-phase and other heterogeneous reactions, including processes like oligomerization. Such processes should be taking place in all seasons. However, during the photochemically active periods (e.g., summer) there are

other chemical pathways (e.g., reactions with OH and ozone) to convert the organic precursors to SOA. Adding to this the increased presence of lower-level clouds during winter and early spring compared to summer in North Hemisphere mid-latitudes (Stubenrauch et al., 2006), one would expect a higher importance of heterogeneous oxidation in winter. Finally, the underprediction of SOA by the model during winter may be also associated with an overestimation of atmospheric removal.

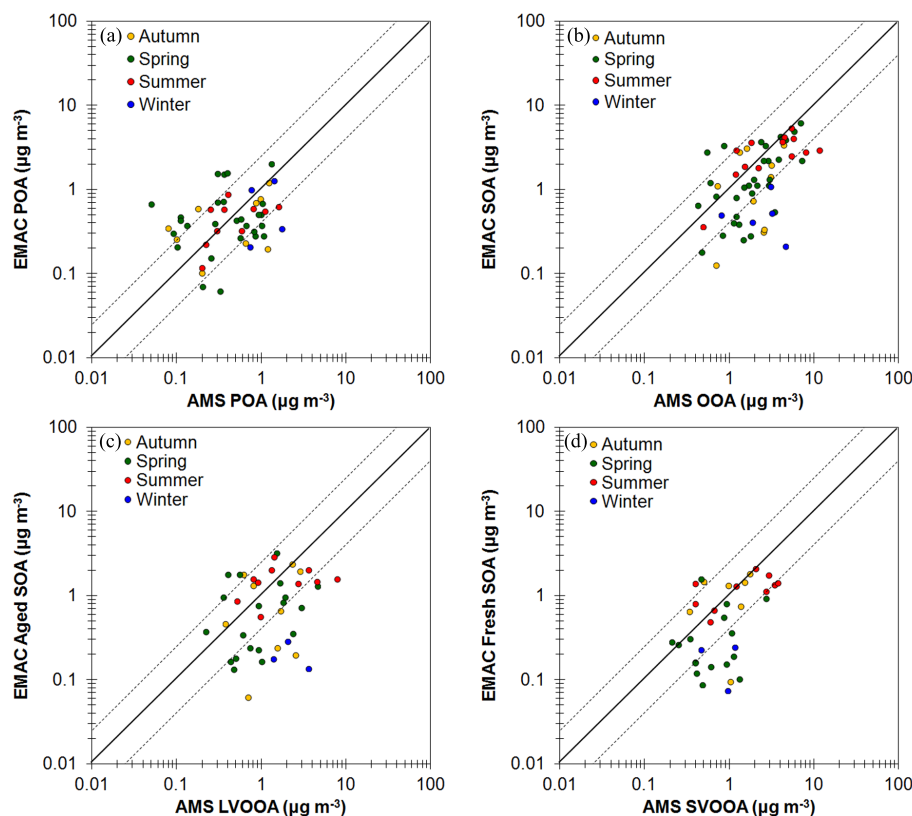


Figure 13. Scatter plots comparing model results to AMS for (a) POA, (b) OOA, (c) LV-OOA, and (d) SV-OOA concentrations (in $\mu\text{g m}^{-3}$) in the Northern Hemisphere during 2001–2010. Each point represents the data set average value and is colored based on the season of the field campaign. Also shown are the 1 : 1, 2 : 1, and 1 : 2 lines.

PMF and EMAC results indicate that aged SOA levels exceed those of fresh SOA during all seasons. The EMAC performance for aged SOA appears to be better during spring (NMB = -33%), summer (NMB = -36%), and autumn (NMB = -32%), and much worse during winter (NMB = -91%) (Table 5; Fig. 13c). The overall performance of the model for fresh SOA (NME = 60% , NMB = -30%) (Table 6, Fig. 13d) appears to be better than aged SOA (NME = 71% , NMB = -40%), which supports our conclusions from the spatial model evaluation that the atmospheric aging of SOA may be underestimated by EMAC. However, this apparent discrepancy may be partially due to our assumption that LV-OOA corresponds only to multiple generational SOA. This is not consistent with recent studies that reported formation of LV-OOA from the first oxidation step of biogenic VOCs (Ehn et al., 2014). During winter, EMAC also underestimates the fresh SOA levels (NMB = -79%). This underprediction of both fresh and aged SOA during winter suggests that one or more important wintertime SOA formation pathways are missing in our model.

5.4 OA composition

According to PMF results, the OOA/OA ratio increases downwind of the urban centers and in rural areas (from 61% over urban environments to 86% over remote areas; Fig. 14a). This is generally consistent with the EMAC predictions. The predicted SOA/OA fraction increases downwind of the urban centers (from 76% over urban locations to 80% over rural areas). This change is lower than the PMF estimates but could be explained by the uncertainty of the PMF analyses (Fig. 14a). Alternatively, this may indicate that EMAC tends to underpredict the aging rate of OA. OOA/OA is consistently high during all seasons (around 80%) with the highest ratio predicted in summer (90%) and the lowest in winter (74%) (Fig. 14b). The model predicts high SOA/OA during all seasons except winter (Fig. 14b). The highest SOA/OA ratio is predicted during summer (87%) when the photo-oxidation of SOA is enhanced. The low SOA/OA during winter (47%) once again shows the inability of the EMAC model to reproduce the observed SOA levels during that season.

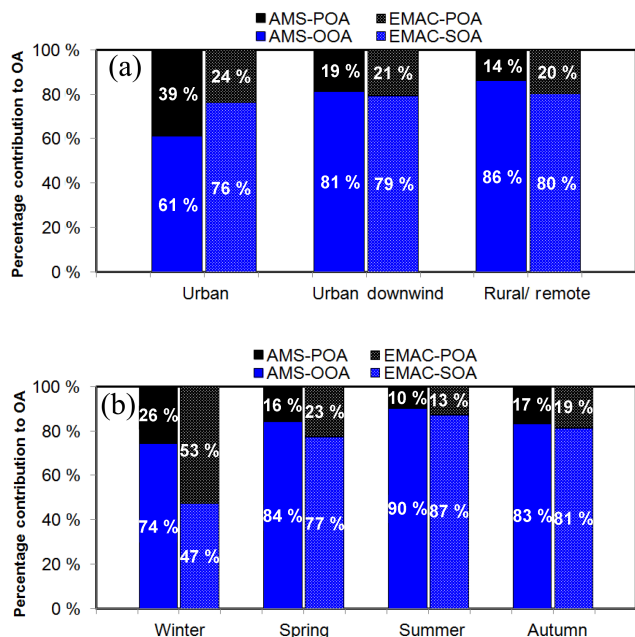


Figure 14. (a) Spatial and (b) seasonal composition of total OA mass calculated from EMAC and AMS results in the Northern Hemisphere during 2001–2010.

Both PMF and EMAC indicate that aged SOA is higher than fresh SOA in all types of environments and seasons (Fig. 15). PMF results suggest that LV-OOA / OOA is higher over urban-downwind environments (69%), while EMAC aged SOA / SOA is similar over all types of locations (59%) (Fig. 15a). The high fresh SOA fraction estimated over rural areas by both PMF and EMAC (around 40%) indicates that fresh SOA production occurs even remotely from the sources. The composition of OOA exhibits a seasonal cycle as well since AMS results indicate that LV-OOA / OOA is higher during winter (73%) and lower during summer (57%) (Fig. 15b). EMAC predicts the highest aged SOA / SOA fraction during spring (68%) and the lowest during winter (53%) without any clear seasonal pattern (Fig. 15b).

6 Conclusions

This study estimates the impact of open biomass burning and anthropogenic combustion emissions (from fossil and biofuels) of SVOCs and IVOCs to global OA budgets and distributions. The EMAC simulations indicate that the tropospheric burden of OA consists of 32% fOA and 30% bbOA. Furthermore, 90% of fOA and 70% of bbOA is predicted to be secondary. These results support recent findings from global studies that have also reported strong contributions of SOA from anthropogenic sources to global OA concentrations (Spracklen et al., 2011; Carslaw et al., 2013; Lee et al., 2013; Tsimpidi et al., 2014).

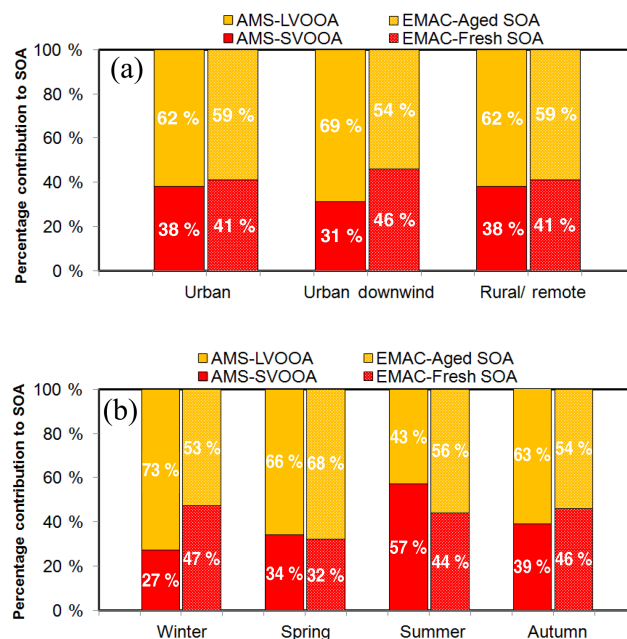


Figure 15. (a) Spatial and (b) seasonal composition of SOA and OOA mass calculated from EMAC and AMS results, respectively, in the Northern Hemisphere during 2001–2010.

The tropospheric burdens of fOA and bbOA follow a clear seasonal pattern. fOA is higher during the boreal summer (0.63 Tg) and lower during winter (0.57 Tg), while bbOA is higher during the dry season in the tropics (1.15 Tg during August) and lower during the wet season (0.17 Tg during April). The simulated spatial distribution of fOA and bbOA is driven by the sources of their precursors and atmospheric transport. Higher fPOA concentrations occur over densely populated and highly industrialized areas of the Northern Hemisphere while further downwind fPOA decreases substantially due to dilution and evaporation. On the other hand, fSOA maintains similar levels downwind of the anthropogenic sources due to the continued chemical transformations. bbPOA concentrations peak over the tropical and the boreal forests while bbSOA has high concentrations over a wide area covering most of South America, central and southern Africa, and Southeast Asia, including Indonesia and even parts of the southern Atlantic Ocean.

AMS results from 84 field campaigns performed at continental locations in the Northern Hemisphere during the examined period (2001–2010) have been used to provide further insights into the composition of OA in three different types of environments: urban, urban-downwind and rural areas, during four seasons. The spatial analysis of AMS and EMAC results indicate that over urban areas POA is highest while further downwind and in rural areas decreases substantially due to dilution and evaporation. On the other hand, SOA is found to be high over all types of environments. This results in an increase of the SOA / OA ratio downwind of the

urban centers. The seasonal analysis of the results does not include the urban areas since the model cannot reproduce the high OA concentrations over urban environments due to its limited spatial resolution. The seasonal evaluation of the model results against the AMS measurements showed a major weakness of the model associated with calculated POA and SOA concentration levels during winter. This indicates that the model is probably missing both an important source and a formation pathway of OA, which becomes increasingly important during boreal winter. Possible causes include the underestimation of residential biofuel emissions during winter, the underestimation of vehicle cold-start emissions, the neglect of aqueous-phase and heterogeneous oxidation reactions in the model, and the overestimation of the atmospheric removal of POA and freshly formed SOA.

AMS results indicate that OA consists of 15 % HOA and 85 % OOA on average during all seasons. EMAC is able to reproduce this dominance of OOA and its results suggest that SOA accounts for 80 % of total OA. At many locations, PMF analysis identified two subtypes of OOA that differ in volatility and oxidation state (LV-OOA and SV-OOA). PMF results indicate that LV-OOA is higher than SV-OOA regardless of the season or the type of environment. The overall LV-OOA/OOA fraction during the four seasons is 63 % according to AMS measurement analysis. Assuming that SV-OOA corresponds to fresh SOA (first generation oxidation products) and LV-OOA corresponds to aged SOA (later generation oxidation products), EMAC is able to reproduce the PMF results predicting a dominance of aged SOA during all seasons (59 % of the total SOA on average).

The Supplement related to this article is available online at doi:10.5194/acp-16-8939-2016-supplement.

Acknowledgements. The research leading to these results has received funding from the European Research Council under the European Union's Seventh Framework Programme (FP7/2007–2013)/ERC grant agreement no. 226144. A. P. Tsimpidi acknowledges support from a DFG individual grand programme (project reference TS 335/2-1) and V. A. Karydis acknowledges support from a FP7 Marie Curie Career Integration Grant (project reference 618349).

The article processing charges for this open-access publication were covered by the Max Planck Society.

Edited by: K. Tsigaridis

Reviewed by: two anonymous referees

References

- Alvarado, M. J., Lonsdale, C. R., Yokelson, R. J., Akagi, S. K., Coe, H., Craven, J. S., Fischer, E. V., McMeeking, G. R., Seinfeld, J. H., Soni, T., Taylor, J. W., Weise, D. R., and Wold, C. E.: Investigating the links between ozone and organic aerosol chemistry in a biomass burning plume from a prescribed fire in California chaparral, *Atmos. Chem. Phys.*, 15, 6667–6688, doi:10.5194/acp-15-6667-2015, 2015.
- Aiken, A. C., Salcedo, D., Cubison, M. J., Huffman, J. A., DeCarlo, P. F., Ulbrich, I. M., Docherty, K. S., Sueper, D., Kimmel, J. R., Worsnop, D. R., Trimborn, A., Northway, M., Stone, E. A., Schauer, J. J., Volkamer, R. M., Fortner, E., de Foy, B., Wang, J., Laskin, A., Shutthanandan, V., Zheng, J., Zhang, R., Gaffney, J., Marley, N. A., Paredes-Miranda, G., Arnott, W. P., Molina, L. T., Sosa, G., and Jimenez, J. L.: Mexico City aerosol analysis during MILAGRO using high resolution aerosol mass spectrometry at the urban supersite (T0) – Part 1: Fine particle composition and organic source apportionment, *Atmos. Chem. Phys.*, 9, 6633–6653, doi:10.5194/acp-9-6633-2009, 2009.
- Aiken, A. C., de Foy, B., Wiedinmyer, C., DeCarlo, P. F., Ulbrich, I. M., Wehrli, M. N., Szidat, S., Prevot, A. S. H., Noda, J., Wacker, L., Volkamer, R., Fortner, E., Wang, J., Laskin, A., Shutthanandan, V., Zheng, J., Zhang, R., Paredes-Miranda, G., Arnott, W. P., Molina, L. T., Sosa, G., Querol, X., and Jimenez, J. L.: Mexico city aerosol analysis during MILAGRO using high resolution aerosol mass spectrometry at the urban supersite (T0) – Part 2: Analysis of the biomass burning contribution and the non-fossil carbon fraction, *Atmos. Chem. Phys.*, 10, 5315–5341, doi:10.5194/acp-10-5315-2010, 2010.
- Athanasopoulou, E., Vogel, H., Vogel, B., Tsimpidi, A. P., Pandis, S. N., Knote, C., and Fountoukis, C.: Modeling the meteorological and chemical effects of secondary organic aerosols during an EUCAARI campaign, *Atmos. Chem. Phys.*, 13, 625–645, doi:10.5194/acp-13-625-2013, 2013.
- Aumont, B., Valorso, R., Mouchel-Vallon, C., Camredon, M., Lee-Taylor, J., and Madronich, S.: Modeling SOA formation from the oxidation of intermediate volatility *n*-alkanes, *Atmos. Chem. Phys.*, 12, 7577–7589, doi:10.5194/acp-12-7577-2012, 2012.
- Bahreini, R., Middlebrook, A. M., de Gouw, J. A., Warneke, C., Trainer, M., Brock, C. A., Stark, H., Brown, S. S., Dube, W. P., Gilman, J. B., Hall, K., Holloway, J. S., Kuster, W. C., Perring, A. E., Prevot, A. S. H., Schwarz, J. P., Spackman, J. R., Szidat, S., Wagner, N. L., Weber, R. J., Zotter, P., and Parrish, D. D.: Gasoline emissions dominate over diesel in formation of secondary organic aerosol mass, *Geophys. Res. Lett.*, 39, L06805, doi:10.1029/2011gl050718, 2012.
- Bergström, R., Denier van der Gon, H. A. C., Prévôt, A. S. H., Yttri, K. E., and Simpson, D.: Modelling of organic aerosols over Europe (2002–2007) using a volatility basis set (VBS) framework: application of different assumptions regarding the formation of secondary organic aerosol, *Atmos. Chem. Phys.*, 12, 8499–8527, doi:10.5194/acp-12-8499-2012, 2012.
- Bougiatioti, A., Stavroulas, I., Kostenidou, E., Zarnmpas, P., Theodosi, C., Kouvarakis, G., Canonaco, F., Prévôt, A. S. H., Nenes, A., Pandis, S. N., and Mihalopoulos, N.: Processing of biomass-burning aerosol in the eastern Mediterranean during summertime, *Atmos. Chem. Phys.*, 14, 4793–4807, doi:10.5194/acp-14-4793-2014, 2014.

- Canagaratna, M. R., Jimenez, J. L., Kroll, J. H., Chen, Q., Kessler, S. H., Massoli, P., Hildebrandt Ruiz, L., Fortner, E., Williams, L. R., Wilson, K. R., Surratt, J. D., Donahue, N. M., Jayne, J. T., and Worsnop, D. R.: Elemental ratio measurements of organic compounds using aerosol mass spectrometry: characterization, improved calibration, and implications, *Atmos. Chem. Phys.*, 15, 253–272, doi:10.5194/acp-15-253-2015, 2015.
- Cappa, C. D. and Wilson, K. R.: Multi-generation gas-phase oxidation, equilibrium partitioning, and the formation and evolution of secondary organic aerosol, *Atmos. Chem. Phys.*, 12, 9505–9528, doi:10.5194/acp-12-9505-2012, 2012.
- Carbone, S., Aurela, M., Saarnio, K., Saarikoski, S., Timonen, H., Frey, A., Sueper, D., Ulbrich, I. M., Jimenez, J. L., Kulmala, M., Worsnop, D. R., and Hillamo, R. E.: Wintertime Aerosol Chemistry in Sub-Arctic Urban Air, *Aerosol Sci. Tech.*, 48, 313–323, 2014.
- Carslaw, K. S., Lee, L. A., Reddington, C. L., Mann, G. W., and Pringle, K. J.: The magnitude and sources of uncertainty in global aerosol, *Faraday Discuss.*, 165, 495–512, 2013.
- Chen, L. W. A., Watson, J. G., Chow, J. C., and Magliano, K. L.: Quantifying PM_{2.5} source contributions for the San Joaquin Valley with multivariate receptor models, *Environ. Sci. Technol.*, 41, 2818–2826, 2007.
- Chen, Q., Farmer, D. K., Rizzo, L. V., Pauliquevis, T., Kuwata, M., Karl, T. G., Guenther, A., Allan, J. D., Coe, H., Andreae, M. O., Pöschl, U., Jimenez, J. L., Artaxo, P., and Martin, S. T.: Submicron particle mass concentrations and sources in the Amazonian wet season (AMAZE-08), *Atmos. Chem. Phys.*, 15, 3687–3701, doi:10.5194/acp-15-3687-2015, 2015.
- Chen, Y., Morton, D. C., Jin, Y., Gollatz, G. J., Kasibhatla, P. S., van der Werf, G. R., DeFries, R. S., and Randerson, J. T.: Long-term trends and interannual variability of forest, savanna and agricultural fires in South America, *Carbon Management*, 4, 617–638, 2013.
- Chirico, R., DeCarlo, P. F., Heringa, M. F., Tritscher, T., Richter, R., Prévôt, A. S. H., Dommen, J., Weingartner, E., Wehrle, G., Gysel, M., Laborde, M., and Baltensperger, U.: Impact of after-treatment devices on primary emissions and secondary organic aerosol formation potential from in-use diesel vehicles: results from smog chamber experiments, *Atmos. Chem. Phys.*, 10, 11545–11563, doi:10.5194/acp-10-11545-2010, 2010.
- Clarke, L., Edmonds, J., Jacoby, H., Pitcher, H., Reilly, J., and Richels, R.: Scenarios of greenhouse gas emissions and atmospheric concentrations (Part A) and review of integrated scenario development and application (Part B), A report by the US climate change science program and the subcommittee on global change research, Department of Energy, Office of Biological & Environmental Research, Washington, D.C., USA, 260 pp., 2007.
- Crippa, M., El Haddad, I., Slowik, J. G., DeCarlo, P. F., Mohr, C., Heringa, M. F., Chirico, R., Marchand, N., Sciare, J., Baltensperger, U., and Prevot, A. S. H.: Identification of marine and continental aerosol sources in Paris using high resolution aerosol mass spectrometry, *J. Geophys. Res.-Atmos.*, 118, 1950–1963, doi:10.1002/jgrd.50151, 2013a.
- Crippa, M., DeCarlo, P. F., Slowik, J. G., Mohr, C., Heringa, M. F., Chirico, R., Poulain, L., Freutel, F., Sciare, J., Cozic, J., Di Marco, C. F., Elsasser, M., Nicolas, J. B., Marchand, N., Abidi, E., Wiedensohler, A., Drewnick, F., Schneider, J., Borrmann, S., Nemitz, E., Zimmermann, R., Jaffrezo, J.-L., Prévôt, A. S. H., and Baltensperger, U.: Wintertime aerosol chemical composition and source apportionment of the organic fraction in the metropolitan area of Paris, *Atmos. Chem. Phys.*, 13, 961–981, doi:10.5194/acp-13-961-2013, 2013b.
- Crippa, M., Canonaco, F., Lanz, V. A., Äijälä, M., Allan, J. D., Carbone, S., Capes, G., Ceburnis, D., Dall’Osto, M., Day, D. A., DeCarlo, P. F., Ehn, M., Eriksson, A., Freney, E., Hildebrandt Ruiz, L., Hillamo, R., Jimenez, J. L., Junninen, H., Kiendler-Scharr, A., Kortelainen, A.-M., Kulmala, M., Laaksonen, A., Mensah, A. A., Mohr, C., Nemitz, E., O’Dowd, C., Ovadnevaite, J., Pandis, S. N., Petäjä, T., Poulain, L., Saarikoski, S., Sellegri, K., Swietlicki, E., Tiitta, P., Worsnop, D. R., Baltensperger, U., and Prévôt, A. S. H.: Organic aerosol components derived from 25 AMS data sets across Europe using a consistent ME-2 based source apportionment approach, *Atmos. Chem. Phys.*, 14, 6159–6176, doi:10.5194/acp-14-6159-2014, 2014.
- DeCarlo, P. F., Ulbrich, I. M., Crouse, J., de Foy, B., Dunlea, E. J., Aiken, A. C., Knapp, D., Weinheimer, A. J., Campos, T., Wennberg, P. O., and Jimenez, J. L.: Investigation of the sources and processing of organic aerosol over the Central Mexican Plateau from aircraft measurements during MILAGRO, *Atmos. Chem. Phys.*, 10, 5257–5280, doi:10.5194/acp-10-5257-2010, 2010.
- Denier van der Gon, H. A. C., Bergström, R., Fountoukis, C., Johansson, C., Pandis, S. N., Simpson, D., and Visschedijk, A. J. H.: Particulate emissions from residential wood combustion in Europe – revised estimates and an evaluation, *Atmos. Chem. Phys.*, 15, 6503–6519, doi:10.5194/acp-15-6503-2015, 2015.
- Donahue, N. M., Robinson, A. L., Stanier, C. O., and Pandis, S. N.: Coupled partitioning, dilution, and chemical aging of semivolatile organics, *Environ. Sci. Technol.*, 40, 2635–2643, 2006.
- Donahue, N. M., Robinson, A. L., and Pandis, S. N.: Atmospheric organic particulate matter: From smoke to secondary organic aerosol, *Atmos. Environ.*, 43, 94–106, 2009.
- Ehn, M., Thornton, J. A., Kleist, E., Sipila, M., Junninen, H., Pullinen, I., Springer, M., Rubach, F., Tillmann, R., Lee, B., Lopez-Hilfiker, F., Andres, S., Acir, I.-H., Rissanen, M., Jokinen, T., Schobesberger, S., Kangasluoma, J., Kontkanen, J., Nieminen, T., Kurten, T., Nielsen, L. B., Jorgensen, S., Kjaergaard, H. G., Canagaratna, M., Maso, M. D., Berndt, T., Petaja, T., Wahner, A., Kerminen, V.-M., Kulmala, M., Worsnop, D. R., Wildt, J., and Mentel, T. F.: A large source of low-volatility secondary organic aerosol, *Nature*, 506, 476–479, doi:10.1038/nature13032, 2014.
- Fountoukis, C., Racherla, P. N., Denier van der Gon, H. A. C., Polymeneas, P., Charalampidis, P. E., Pilinis, C., Wiedensohler, A., Dall’Osto, M., O’Dowd, C., and Pandis, S. N.: Evaluation of a three-dimensional chemical transport model (PMCAMx) in the European domain during the EUCAARI May 2008 campaign, *Atmos. Chem. Phys.*, 11, 10331–10347, doi:10.5194/acp-11-10331-2011, 2011.
- Fountoukis, C., Megaritis, A. G., Skyllakou, K., Charalampidis, P. E., Pilinis, C., Denier van der Gon, H. A. C., Crippa, M., Canonaco, F., Mohr, C., Prévôt, A. S. H., Allan, J. D., Poulain, L., Petäjä, T., Tiitta, P., Carbone, S., Kiendler-Scharr, A., Nemitz, E., O’Dowd, C., Swietlicki, E., and Pandis, S. N.: Organic aerosol concentration and composition over Europe: insights from comparison of regional model predictions with aerosol mass spec-

- trometer factor analysis, *Atmos. Chem. Phys.*, 14, 9061–9076, doi:10.5194/acp-14-9061-2014, 2014.
- Fountoukis, C., Megaritis, A. G., Skyllakou, K., Charalampidis, P. E., Denier van der Gon, H. A. C., Crippa, M., Prévôt, A. S. H., Fachinger, F., Wiedensohler, A., Pilinis, C., and Pandis, S. N.: Simulating the formation of carbonaceous aerosol in a European Megacity (Paris) during the MEGAPOLI summer and winter campaigns, *Atmos. Chem. Phys.*, 16, 3727–3741, doi:10.5194/acp-16-3727-2016, 2016.
- Ge, X., Setyan, A., Sun, Y., and Zhang, Q.: Primary and secondary organic aerosols in Fresno, California during wintertime: Results from high resolution aerosol mass spectrometry, *J. Geophys. Res.-Atmos.*, 117, D19301, doi:10.1029/2012jd018026, 2012.
- Gentner, D. R., Isaacman, G., Worton, D. R., Chan, A. W. H., Dallmann, T. R., Davis, L., Liu, S., Day, D. A., Russell, L. M., Wilson, K. R., Weber, R., Guha, A., Harley, R. A., and Goldstein, A. H.: Elucidating secondary organic aerosol from diesel and gasoline vehicles through detailed characterization of organic carbon emissions, *P. Natl. Acad. Sci. USA*, 109, 18318–18323, 2012.
- Goldstein, A. H. and Galbally, I. E.: Known and unexplored organic constituents in the earth's atmosphere, *Environ. Sci. Technol.*, 41, 1514–1521, 2007.
- Gordon, T. D., Presto, A. A., May, A. A., Nguyen, N. T., Lipsky, E. M., Donahue, N. M., Gutierrez, A., Zhang, M., Madrox, C., Rieger, P., Chattopadhyay, S., Maldonado, H., Maricq, M. M., and Robinson, A. L.: Secondary organic aerosol formation exceeds primary particulate matter emissions for light-duty gasoline vehicles, *Atmos. Chem. Phys.*, 14, 4661–4678, doi:10.5194/acp-14-4661-2014, 2014.
- Grieshop, A. P., Logue, J. M., Donahue, N. M., and Robinson, A. L.: Laboratory investigation of photochemical oxidation of organic aerosol from wood fires 1: measurement and simulation of organic aerosol evolution, *Atmos. Chem. Phys.*, 9, 1263–1277, doi:10.5194/acp-9-1263-2009, 2009.
- Hayes, P. L., Ortega, A. M., Cubison, M. J., Froyd, K. D., Zhao, Y., Cliff, S. S., Hu, W. W., Toohey, D. W., Flynn, J. H., Lefer, B. L., Grossberg, N., Alvarez, S., Rappenglueck, B., Taylor, J. W., Allan, J. D., Holloway, J. S., Gilman, J. B., Kuster, W. C., De Gouw, J. A., Massoli, P., Zhang, X., Liu, J., Weber, R. J., Corrigan, A. L., Russell, L. M., Isaacman, G., Worton, D. R., Kreisberg, N. M., Goldstein, A. H., Thalman, R., Waxman, E. M., Volkamer, R., Lin, Y. H., Surratt, J. D., Kleindienst, T. E., Offenberg, J. H., Dusanter, S., Griffith, S., Stevens, P. S., Brioude, J., Angevine, W. M., and Jimenez, J. L.: Organic aerosol composition and sources in Pasadena, California, during the 2010 CalNex campaign, *J. Geophys. Res.-Atmos.*, 118, 9233–9257, doi:10.1002/jgrd.50530, 2013.
- Henze, D. K., Seinfeld, J. H., Ng, N. L., Kroll, J. H., Fu, T.-M., Jacob, D. J., and Heald, C. L.: Global modeling of secondary organic aerosol formation from aromatic hydrocarbons: high- vs. low-yield pathways, *Atmos. Chem. Phys.*, 8, 2405–2420, doi:10.5194/acp-8-2405-2008, 2008.
- Hodzic, A., Jimenez, J. L., Madronich, S., Canagaratna, M. R., DeCarlo, P. F., Kleinman, L., and Fast, J.: Modeling organic aerosols in a megacity: potential contribution of semi-volatile and intermediate volatility primary organic compounds to secondary organic aerosol formation, *Atmos. Chem. Phys.*, 10, 5491–5514, doi:10.5194/acp-10-5491-2010, 2010.
- Hodzic, A., Kasibhatla, P. S., Jo, D. S., Cappa, C. D., Jimenez, J. L., Madronich, S., and Park, R. J.: Rethinking the global secondary organic aerosol (SOA) budget: stronger production, faster removal, shorter lifetime, *Atmos. Chem. Phys.*, 16, 7917–7941, doi:10.5194/acp-16-7917-2016, 2016.
- Hu, W. W., Campuzano-Jost, P., Palm, B. B., Day, D. A., Ortega, A. M., Hayes, P. L., Krechmer, J. E., Chen, Q., Kuwata, M., Liu, Y. J., de Sá, S. S., McKinney, K., Martin, S. T., Hu, M., Budisulistiorini, S. H., Riva, M., Surratt, J. D., St. Clair, J. M., Isaacman-Van Wertz, G., Yee, L. D., Goldstein, A. H., Carbone, S., Brito, J., Artaxo, P., de Gouw, J. A., Koss, A., Wisthaler, A., Mikoviny, T., Karl, T., Kaser, L., Jud, W., Hansel, A., Docherty, K. S., Alexander, M. L., Robinson, N. H., Coe, H., Allan, J. D., Canagaratna, M. R., Paulot, F., and Jimenez, J. L.: Characterization of a real-time tracer for isoprene epoxydiols-derived secondary organic aerosol (IEPOX-SOA) from aerosol mass spectrometer measurements, *Atmos. Chem. Phys.*, 15, 11807–11833, doi:10.5194/acp-15-11807-2015, 2015.
- IPCC – Intergovernmental Panel on Climate Change: The physical science basis, in: Contribution of working group I to the fifth assessment report of the intergovernmental panel on climate change, edited by: Stocker, T. F., Qin, D., Plattner, G.-K., Tignor, M., Allen, S. K., Boschung, J., Nauels, A., Xia, Y., Bex, V., and Midgley, P. M., Cambridge University Press, Cambridge, UK and New York, NY, USA, 2013.
- Jathar, S. H., Farina, S. C., Robinson, A. L., and Adams, P. J.: The influence of semi-volatile and reactive primary emissions on the abundance and properties of global organic aerosol, *Atmos. Chem. Phys.*, 11, 7727–7746, doi:10.5194/acp-11-7727-2011, 2011.
- Jimenez, J. L., Jayne, J. T., Shi, Q., Kolb, C. E., Worsnop, D. R., Yourshaw, I., Seinfeld, J. H., Flagan, R. C., Zhang, X. F., Smith, K. A., Morris, J. W., and Davidovits, P.: Ambient aerosol sampling using the Aerodyne Aerosol Mass Spectrometer, *J. Geophys. Res. Atmos.*, 108, 8425, doi:10.1029/2001jd001213, 2003.
- Jimenez, J. L., Canagaratna, M. R., Donahue, N. M., Prevot, A. S. H., Zhang, Q., Kroll, J. H., DeCarlo, P. F., Allan, J. D., Coe, H., Ng, N. L., Aiken, A. C., Docherty, K. S., Ulbrich, I. M., Grieshop, A. P., Robinson, A. L., Duplissy, J., Smith, J. D., Wilson, K. R., Lanz, V. A., Hueglin, C., Sun, Y. L., Tian, J., Laaksonen, A., Raatikainen, T., Rautiainen, J., Vaattovaara, P., Ehn, M., Kulmala, M., Tomlinson, J. M., Collins, D. R., Cubison, M. J., Dunlea, E. J., Huffman, J. A., Onasch, T. B., Alfarra, M. R., Williams, P. I., Bower, K., Kondo, Y., Schneider, J., Drewnick, F., Borrmann, S., Weimer, S., Demerjian, K., Salcedo, D., Cottrell, L., Griffin, R., Takami, A., Miyoshi, T., Hatakeyama, S., Shimojo, A., Sun, J. Y., Zhang, Y. M., Dzepina, K., Kimmel, J. R., Sueper, D., Jayne, J. T., Herndon, S. C., Trimborn, A. M., Williams, L. R., Wood, E. C., Middlebrook, A. M., Kolb, C. E., Baltensperger, U., and Worsnop, D. R.: Evolution of organic aerosols in the atmosphere, *Science*, 326, 1525–1529, 2009.
- Jöckel, P., Tost, H., Pozzer, A., Brühl, C., Buchholz, J., Ganzeveld, L., Hoor, P., Kerkweg, A., Lawrence, M. G., Sander, R., Steil, B., Stiller, G., Tanarhte, M., Taraborrelli, D., van Aardenne, J., and Lelieveld, J.: The atmospheric chemistry general circulation model ECHAM5/MESy1: consistent simulation of ozone from the surface to the mesosphere, *Atmos. Chem. Phys.*, 6, 5067–5104, doi:10.5194/acp-6-5067-2006, 2006.

- Kanakidou, M., Seinfeld, J. H., Pandis, S. N., Barnes, I., Dentener, F. J., Facchini, M. C., Van Dingenen, R., Ervens, B., Nenes, A., Nielsen, C. J., Swietlicki, E., Putaud, J. P., Balkanski, Y., Fuzzi, S., Horth, J., Moortgat, G. K., Winterhalter, R., Myhre, C. E. L., Tsigaridis, K., Vignati, E., Stephanou, E. G., and Wilson, J.: Organic aerosol and global climate modelling: a review, *Atmos. Chem. Phys.*, 5, 1053–1123, doi:10.5194/acp-5-1053-2005, 2005.
- Karydis, V. A., Tsimpidi, A. P., Pozzer, A., Astitha, M., and Lelieveld, J.: Effects of mineral dust on global atmospheric nitrate concentrations, *Atmos. Chem. Phys.*, 16, 1491–1509, doi:10.5194/acp-16-1491-2016, 2016.
- Kerkweg, A., Buchholz, J., Ganzeveld, L., Pozzer, A., Tost, H., and Jöckel, P.: Technical Note: An implementation of the dry removal processes DRY DEPosition and SEDimentation in the Modular Earth Submodel System (MESSy), *Atmos. Chem. Phys.*, 6, 4617–4632, doi:10.5194/acp-6-4617-2006, 2006a.
- Kerkweg, A., Sander, R., Tost, H., and Jöckel, P.: Technical note: Implementation of prescribed (OFFLEM), calculated (ONLEM), and pseudo-emissions (TNUDGE) of chemical species in the Modular Earth Submodel System (MESSy), *Atmos. Chem. Phys.*, 6, 3603–3609, doi:10.5194/acp-6-3603-2006, 2006b.
- Kopacz, M., Jacob, D. J., Fisher, J. A., Logan, J. A., Zhang, L., Megretskaia, I. A., Yantosca, R. M., Singh, K., Henze, D. K., Burrows, J. P., Buchwitz, M., Khlystova, I., McMillan, W. W., Gille, J. C., Edwards, D. P., Eldering, A., Thouret, V., and Nedelec, P.: Global estimates of CO sources with high resolution by adjoint inversion of multiple satellite datasets (MOPITT, AIRS, SCIAMACHY, TES), *Atmos. Chem. Phys.*, 10, 855–876, doi:10.5194/acp-10-855-2010, 2010.
- Kostenidou, E., Kaltsonoudis, C., Tsiflikiotou, M., Louvaris, E., Russell, L. M., and Pandis, S. N.: Burning of olive tree branches: a major organic aerosol source in the Mediterranean, *Atmos. Chem. Phys.*, 13, 8797–8811, doi:10.5194/acp-13-8797-2013, 2013.
- Kroll, J. H. and Seinfeld, J. H.: Chemistry of secondary organic aerosol: Formation and evolution of low-volatility organics in the atmosphere, *Atmos. Environ.*, 42, 3593–3624, 2008.
- Lanz, V. A., Alfarra, M. R., Baltensperger, U., Buchmann, B., Hueglin, C., and Prévôt, A. S. H.: Source apportionment of submicron organic aerosols at an urban site by factor analytical modelling of aerosol mass spectra, *Atmos. Chem. Phys.*, 7, 1503–1522, doi:10.5194/acp-7-1503-2007, 2007.
- Lanz, V. A., Alfarra, M. R., Baltensperger, U., Buchmann, B., Hueglin, C., Szidat, S., Wehrli, M. N., Wacker, L., Weimer, S., Caseiro, A., Puxbaum, H., and Prevot, A. S. H.: Source attribution of submicron organic aerosols during wintertime inversions by advanced factor analysis of aerosol mass spectra, *Environ. Sci. Technol.*, 42, 214–220, 2008.
- Lanz, V. A., Prévôt, A. S. H., Alfarra, M. R., Weimer, S., Mohr, C., DeCarlo, P. F., Gianini, M. F. D., Hueglin, C., Schneider, J., Favez, O., D'Anna, B., George, C., and Baltensperger, U.: Characterization of aerosol chemical composition with aerosol mass spectrometry in Central Europe: an overview, *Atmos. Chem. Phys.*, 10, 10453–10471, doi:10.5194/acp-10-10453-2010, 2010.
- Lauer, A., Eyring, V., Hendricks, J., Jöckel, P., and Lohmann, U.: Global model simulations of the impact of ocean-going ships on aerosols, clouds, and the radiation budget, *Atmos. Chem. Phys.*, 7, 5061–5079, doi:10.5194/acp-7-5061-2007, 2007.
- Lee, L. A., Pringle, K. J., Reddington, C. L., Mann, G. W., Stier, P., Spracklen, D. V., Pierce, J. R., and Carslaw, K. S.: The magnitude and causes of uncertainty in global model simulations of cloud condensation nuclei, *Atmos. Chem. Phys.*, 13, 8879–8914, doi:10.5194/acp-13-8879-2013, 2013.
- Lelieveld, J., Barlas, C., Giannadaki, D., and Pozzer, A.: Model calculated global, regional and megacity premature mortality due to air pollution, *Atmos. Chem. Phys.*, 13, 7023–7037, doi:10.5194/acp-13-7023-2013, 2013.
- Lelieveld, J., Evans, J. S., Fnais, M., Giannadaki, D., and Pozzer, A.: The contribution of outdoor air pollution sources to premature mortality on a global scale, *Nature*, 525, 367–371, doi:10.1038/nature15371, 2015.
- Marcolli, C., Canagaratna, M. R., Worsnop, D. R., Bahreini, R., de Gouw, J. A., Warneke, C., Goldan, P. D., Kuster, W. C., Williams, E. J., Lerner, B. M., Roberts, J. M., Meagher, J. F., Fehsenfeld, F. C., Marchewka, M., Bertman, S. B., and Middlebrook, A. M.: Cluster Analysis of the Organic Peaks in Bulk Mass Spectra Obtained During the 2002 New England Air Quality Study with an Aerodyne Aerosol Mass Spectrometer, *Atmos. Chem. Phys.*, 6, 5649–5666, doi:10.5194/acp-6-5649-2006, 2006.
- May, A. A., Levin, E. J. T., Hennigan, C. J., Riipinen, I., Lee, T., Collett, J. L., Jimenez, J. L., Kreidenweis, S. M., and Robinson, A. L.: Gas-particle partitioning of primary organic aerosol emissions: 3. Biomass burning, *J. Geophys. Res.-Atmos.*, 118, 11327–11338, doi:10.1002/jgrd.50828, 2013.
- May, A. A., Nguyen, N. T., Presto, A. A., Gordon, T. D., Lipsky, E. M., Karve, M., Gutierrez, A., Robertson, W. H., Zhang, M., Brandow, C., Chang, O., Chen, S., Cicero-Fernandez, P., Dinkins, L., Fuentes, M., Huang, S.-M., Ling, R., Long, J., Maddox, C., Massetti, J., McCauley, E., Miguel, A., Na, K., Ong, R., Pang, Y., Rieger, P., Sax, T., Tin, T., Thu, V., Chattopadhyay, S., Maldonado, H., Maricq, M. M., and Robinson, A. L.: Gas- and particle-phase primary emissions from in-use, on-road gasoline and diesel vehicles, *Atmos. Environ.*, 88, 247–260, doi:10.1016/j.atmosenv.2014.01.046, 2014.
- McFiggans, G., Artaxo, P., Baltensperger, U., Coe, H., Facchini, M. C., Feingold, G., Fuzzi, S., Gysel, M., Laaksonen, A., Lohmann, U., Mentel, T. F., Murphy, D. M., O'Dowd, C. D., Snider, J. R., and Weingartner, E.: The effect of physical and chemical aerosol properties on warm cloud droplet activation, *Atmos. Chem. Phys.*, 6, 2593–2649, doi:10.5194/acp-6-2593-2006, 2006.
- Miracolo, M. A., Hennigan, C. J., Ranjan, M., Nguyen, N. T., Gordon, T. D., Lipsky, E. M., Presto, A. A., Donahue, N. M., and Robinson, A. L.: Secondary aerosol formation from photochemical aging of aircraft exhaust in a smog chamber, *Atmos. Chem. Phys.*, 11, 4135–4147, doi:10.5194/acp-11-4135-2011, 2011.
- Mohr, C., DeCarlo, P. F., Heringa, M. F., Chirico, R., Slowik, J. G., Richter, R., Reche, C., Alastuey, A., Querol, X., Seco, R., Peñuelas, J., Jiménez, J. L., Crippa, M., Zimmermann, R., Baltensperger, U., and Prévôt, A. S. H.: Identification and quantification of organic aerosol from cooking and other sources in Barcelona using aerosol mass spectrometer data, *Atmos. Chem. Phys.*, 12, 1649–1665, doi:10.5194/acp-12-1649-2012, 2012.
- Murphy, B. N. and Pandis, S. N.: Simulating the formation of semivolatile primary and secondary organic aerosol in a regional chemical transport model, *Environ. Sci. Technol.*, 43, 4722–4728, 2009.

- Nemitz, E., Jimenez, J. L., Huffman, J. A., Ulbrich, I. M., Canagaratna, M. R., Worsnop, D. R., and Guenther, A. B.: An eddy-covariance system for the measurement of surface/atmosphere exchange fluxes of submicron aerosol chemical species – First application above an urban area, *Aerosol Sci. Tech.*, 42, 636–657, 2008.
- Ng, N. L., Canagaratna, M. R., Jimenez, J. L., Zhang, Q., Ulbrich, I. M., and Worsnop, D. R.: Real-Time Methods for Estimating Organic Component Mass Concentrations from Aerosol Mass Spectrometer Data, *Environ. Sci. Technol.*, 45, 910–916, 2011.
- Paatero, P.: Least squares formulation of robust non-negative factor analysis, *Chemometr. Intel. Lab. Syst.*, 37, 23–35, 1997.
- Paatero, P. and Tapper, U.: Positive matrix factorization-A nonnegative factor model with optimal utilization of error-estimates of data values, *Environmetrics*, 5, 111–126, 1994.
- Poschl, U.: Atmospheric aerosols: Composition, transformation, climate and health effects, *Angew. Chem.-Int. Edit.*, 44, 7520–7540, 2005.
- Pozzer, A., Zimmermann, P., Doering, U. M., van Aardenne, J., Tost, H., Dentener, F., Janssens-Maenhout, G., and Lelieveld, J.: Effects of business-as-usual anthropogenic emissions on air quality, *Atmos. Chem. Phys.*, 12, 6915–6937, doi:10.5194/acp-12-6915-2012, 2012a.
- Pozzer, A., de Meij, A., Pringle, K. J., Tost, H., Doering, U. M., van Aardenne, J., and Lelieveld, J.: Distributions and regional budgets of aerosols and their precursors simulated with the EMAC chemistry-climate model, *Atmos. Chem. Phys.*, 12, 961–987, doi:10.5194/acp-12-961-2012, 2012b.
- Pringle, K. J., Tost, H., Message, S., Steil, B., Giannadaki, D., Nenes, A., Fountoukis, C., Stier, P., Vignati, E., and Lelieveld, J.: Description and evaluation of GMXe: a new aerosol submodel for global simulations (v1), *Geosci. Model Dev.*, 3, 391–412, doi:10.5194/gmd-3-391-2010, 2010.
- Pye, H. O. T. and Seinfeld, J. H.: A global perspective on aerosol from low-volatility organic compounds, *Atmos. Chem. Phys.*, 10, 4377–4401, doi:10.5194/acp-10-4377-2010, 2010.
- Ranjan, M., Presto, A. A., May, A. A., and Robinson, A. L.: Temperature Dependence of Gas-Particle Partitioning of Primary Organic Aerosol Emissions from a Small Diesel Engine, *Aerosol Sci. Tech.*, 46, 13–21, doi:10.1080/02786826.2011.602761, 2012.
- Robinson, A. L., Donahue, N. M., Shrivastava, M. K., Weitkamp, E. A., Sage, A. M., Grieshop, A. P., Lane, T. E., Pierce, J. R., and Pandis, S. N.: Rethinking organic aerosols: Semivolatile emissions and photochemical aging, *Science*, 315, 1259–1262, 2007.
- Robinson, A. L., Grieshop, A. P., Donahue, N. M., and Hunt, S. W.: Updating the conceptual model for fine particle mass emissions from combustion systems, *J. Air Waste Manage.*, 60, 1204–1222, 2010.
- Samy, S. and Zielinska, B.: Secondary organic aerosol production from modern diesel engine emissions, *Atmos. Chem. Phys.*, 10, 609–625, doi:10.5194/acp-10-609-2010, 2010.
- Sander, R., Baumgaertner, A., Gromov, S., Harder, H., Jöckel, P., Kerkweg, A., Kubistin, D., Regelin, E., Riede, H., Sandu, A., Taraborrelli, D., Tost, H., and Xie, Z.-Q.: The atmospheric chemistry box model CAABA/MECCA-3.0, *Geosci. Model Dev.*, 4, 373–380, doi:10.5194/gmd-4-373-2011, 2011.
- Shrivastava, M. K., Lane, T. E., Donahue, N. M., Pandis, S. N., and Robinson, A. L.: Effects of gas particle partitioning and aging of primary emissions on urban and regional organic aerosol concentrations, *J. Geophys. Res.-Atmos.*, 113, D18301, doi:10.1029/2007jd009735, 2008.
- Shrivastava, M., Fast, J., Easter, R., Gustafson Jr., W. I., Zaveri, R. A., Jimenez, J. L., Saide, P., and Hodzic, A.: Modeling organic aerosols in a megacity: comparison of simple and complex representations of the volatility basis set approach, *Atmos. Chem. Phys.*, 11, 6639–6662, doi:10.5194/acp-11-6639-2011, 2011.
- Shrivastava, M., Easter, R. C., Liu, X., Zelenyuk, A., Singh, B., Zhang, K., Ma, P.-L., Chand, D., Ghan, S., Jimenez, J. L., Zhang, Q., Fast, J., Rasch, P. J., and Tiitta, P.: Global transformation and fate of SOA: Implications of low-volatility SOA and gas-phase fragmentation reactions, *J. Geophys. Res.-Atmos.*, 120, 4169–4195, doi:10.1002/2014JD022563, 2015.
- Spracklen, D. V., Jimenez, J. L., Carslaw, K. S., Worsnop, D. R., Evans, M. J., Mann, G. W., Zhang, Q., Canagaratna, M. R., Allan, J., Coe, H., McFiggans, G., Rap, A., and Forster, P.: Aerosol mass spectrometer constraint on the global secondary organic aerosol budget, *Atmos. Chem. Phys.*, 11, 12109–12136, doi:10.5194/acp-11-12109-2011, 2011.
- Stone, E. A., Zhou, J., Snyder, D. C., Rutter, A. P., Mieritz, M., and Schauer, J. J.: A Comparison of Summertime Secondary Organic Aerosol Source Contributions at Contrasting Urban Locations, *Environ. Sci. Technol.*, 43, 3448–3454, 2009.
- Stubenrauch, C. J., Chedin, A., Radel, G., Scott, N. A., and Serrar, S.: Cloud properties and their seasonal and diurnal variability from TOVS path-B, *J. Climate*, 19, 5531–5553, doi:10.1175/jcli3929.1, 2006.
- Suess, D. T. and Prather, K. A.: Mass spectrometry of aerosols, *Chem. Rev.*, 99, 3007–3035, 1999.
- Sun, Y.-L., Zhang, Q., Schwab, J. J., Demerjian, K. L., Chen, W.-N., Bae, M.-S., Hung, H.-M., Hogrefe, O., Frank, B., Rattigan, O. V., and Lin, Y.-C.: Characterization of the sources and processes of organic and inorganic aerosols in New York city with a high-resolution time-of-flight aerosol mass spectrometer, *Atmos. Chem. Phys.*, 11, 1581–1602, doi:10.5194/acp-11-1581-2011, 2011.
- Takegawa, N., Miyazaki, Y., Kondo, Y., Komazaki, Y., Miyakawa, T., Jimenez, J. L., Jayne, J. T., Worsnop, D. R., Allan, J. D., and Weber, R. J.: Characterization of an Aerodyne Aerosol Mass Spectrometer (AMS): Intercomparison with other aerosol instruments, *Aerosol Sci. Tech.*, 39, 760–770, 2005.
- Tost, H., Jöckel, P., Kerkweg, A., Sander, R., and Lelieveld, J.: Technical note: A new comprehensive SCAVenging submodel for global atmospheric chemistry modelling, *Atmos. Chem. Phys.*, 6, 565–574, doi:10.5194/acp-6-565-2006, 2006.
- Tsigaridis, K., Daskalakis, N., Kanakidou, M., Adams, P. J., Artaxo, P., Bahadur, R., Balkanski, Y., Bauer, S. E., Bellouin, N., Benedetti, A., Bergman, T., Berntsen, T. K., Beukes, J. P., Bian, H., Carslaw, K. S., Chin, M., Curci, G., Diehl, T., Easter, R. C., Ghan, S. J., Gong, S. L., Hodzic, A., Hoyle, C. R., Iversen, T., Jathar, S., Jimenez, J. L., Kaiser, J. W., Kirkevåg, A., Koch, D., Kokkola, H., Lee, Y. H., Lin, G., Liu, X., Luo, G., Ma, X., Mann, G. W., Mihalopoulos, N., Morcrette, J.-J., Müller, J.-F., Myhre, G., Myriokefalitakis, S., Ng, N. L., O'Donnell, D., Penner, J. E., Pozzoli, L., Pringle, K. J., Russell, L. M., Schulz, M., Sciare, J., Seland, Ø., Shindell, D. T., Sillman, S., Skeie, R. B., Spracklen, D., Stavrou, T., Steenrod, S. D., Takemura, T., Tiitta, P., Tilmes, S., Tost, H., van Noije, T., van Zyl, P. G., von

- Salzen, K., Yu, F., Wang, Z., Wang, Z., Zaveri, R. A., Zhang, H., Zhang, K., Zhang, Q., and Zhang, X.: The AeroCom evaluation and intercomparison of organic aerosol in global models, *Atmos. Chem. Phys.*, 14, 10845–10895, doi:10.5194/acp-14-10845-2014, 2014.
- Tsimpidi, A. P., Karydis, V. A., Zavala, M., Lei, W., Molina, L., Ulbrich, I. M., Jimenez, J. L., and Pandis, S. N.: Evaluation of the volatility basis-set approach for the simulation of organic aerosol formation in the Mexico City metropolitan area, *Atmos. Chem. Phys.*, 10, 525–546, doi:10.5194/acp-10-525-2010, 2010.
- Tsimpidi, A. P., Karydis, V. A., Zavala, M., Lei, W., Bei, N., Molina, L., and Pandis, S. N.: Sources and production of organic aerosol in Mexico City: insights from the combination of a chemical transport model (PMCAMx-2008) and measurements during MLAGRO, *Atmos. Chem. Phys.*, 11, 5153–5168, doi:10.5194/acp-11-5153-2011, 2011.
- Tsimpidi, A. P., Karydis, V. A., Pozzer, A., Pandis, S. N., and Lelieveld, J.: ORACLE (v1.0): module to simulate the organic aerosol composition and evolution in the atmosphere, *Geosci. Model Dev.*, 7, 3153–3172, doi:10.5194/gmd-7-3153-2014, 2014.
- Ulbrich, I. M., Canagaratna, M. R., Zhang, Q., Worsnop, D. R., and Jimenez, J. L.: Interpretation of organic components from Positive Matrix Factorization of aerosol mass spectrometric data, *Atmos. Chem. Phys.*, 9, 2891–2918, doi:10.5194/acp-9-2891-2009, 2009.
- van der Werf, G. R., Randerson, J. T., Giglio, L., Collatz, G. J., Mu, M., Kasibhatla, P. S., Morton, D. C., DeFries, R. S., Jin, Y., and van Leeuwen, T. T.: Global fire emissions and the contribution of deforestation, savanna, forest, agricultural, and peat fires (1997–2009), *Atmos. Chem. Phys.*, 10, 11707–11735, doi:10.5194/acp-10-11707-2010, 2010.
- Wang, Q., Shao, M., Liu, Y., William, K., Paul, G., Li, X., Liu, Y., and Lu, S.: Impact of biomass burning on urban air quality estimated by organic tracers: Guangzhou and Beijing as cases, *Atmos. Environ.*, 41, 8380–8390, doi:10.1016/j.atmosenv.2007.06.048, 2007.
- Weilenmann, M., Favez, J.-Y., and Alvarez, R.: Cold-start emissions of modern passenger cars at different low ambient temperatures and their evolution over vehicle legislation categories, *Atmos. Environ.*, 43, 2419–2429, 2009.
- Westerholm, R., Christensen, A., and Rosen, A.: Regulated and unregulated exhaust emissions from two three-way catalyst equipped gasoline fuelled vehicles, *Atmos. Environ.*, 30, 3529–3536, 1996.
- Zhang, Q., Alfarra, M. R., Worsnop, D. R., Allan, J. D., Coe, H., Canagaratna, M. R., and Jimenez, J. L.: Deconvolution and quantification of hydrocarbon-like and oxygenated organic aerosols based on aerosol mass spectrometry, *Environ. Sci. Technol.*, 39, 4938–4952, 2005a.
- Zhang, Q., Canagaratna, M. R., Jayne, J. T., Worsnop, D. R., and Jimenez, J. L.: Time- and size-resolved chemical composition of submicron particles in Pittsburgh: Implications for aerosol sources and processes, *J. Geophys. Res.-Atmos.*, 110, D07S09, doi:10.1029/2004jd004649, 2005b.
- Zhang, Q., Jimenez, J. L., Canagaratna, M. R., Allan, J. D., Coe, H., Ulbrich, I., Alfarra, M. R., Takami, A., Middlebrook, A. M., Sun, Y. L., Dzepina, K., Dunlea, E., Docherty, K., DeCarlo, P. F., Salcedo, D., Onasch, T., Jayne, J. T., Miyoshi, T., Shimojo, A., Hatakeyama, S., Takegawa, N., Kondo, Y., Schneider, J., Drewnick, F., Borrmann, S., Weimer, S., Demerjian, K., Williams, P., Bower, K., Bahreini, R., Cottrell, L., Griffin, R. J., Rautiainen, J., Sun, J. Y., Zhang, Y. M., and Worsnop, D. R.: Ubiquity and dominance of oxygenated species in organic aerosols in anthropogenically-influenced Northern Hemisphere midlatitudes, *Geophys. Res. Lett.*, 34, D07S09, doi:10.1029/2007gl029979, 2007.
- Zhang, Q., Jimenez, J. L., Canagaratna, M. R., Ulbrich, I. M., Ng, N. L., Worsnop, D. R., and Sun, Y. L.: Understanding atmospheric organic aerosols via factor analysis of aerosol mass spectrometry: a review, *Anal. Bioanal. Chem.*, 401, 3045–3067, 2011.
- Zhang, Q. J., Beekmann, M., Drewnick, F., Freutel, F., Schneider, J., Crippa, M., Prevot, A. S. H., Baltensperger, U., Poulain, L., Wiedensohler, A., Sciare, J., Gros, V., Borbon, A., Colomb, A., Michoud, V., Doussin, J.-F., Denier van der Gon, H. A. C., Haffelin, M., Dupont, J.-C., Siour, G., Petetin, H., Bessagnet, B., Pandis, S. N., Hodzic, A., Sanchez, O., Honoré, C., and Perrussel, O.: Formation of organic aerosol in the Paris region during the MEGAPOLI summer campaign: evaluation of the volatility-basis-set approach within the CHIMERE model, *Atmos. Chem. Phys.*, 13, 5767–5790, doi:10.5194/acp-13-5767-2013, 2013.